

OGPO: Sample Efficient Full-Finetuning of Generative Control Policies

Sarvesh Patil^{a,§}, Mitsuhiro Nakamoto^{b,§}, Manan Agarwal^{a,‡}, Shashwat Saxena^{a,‡}, Jesse Zhang^{c,‡}, Giri Anantharaman^a, Cleah Winston^c, Chaoyi Pan^a, Douglas Chen^a, Nai-Chieh Huang^a, Zeynep Temel^a, Oliver Kroemer^a, Abhishek Gupta^{cd}, Sergey Levine^b, Hongkai Dai^{d,†}, Paarth Shah^{d,†}, Max Simchowitz^{a,†},

[§]Project lead. [‡]Equal Contribution. [†]Equal advising.

^aCarnegie Mellon University ^bUniversity of California, Berkeley ^cUniversity of Washington

^dToyota Research Institute

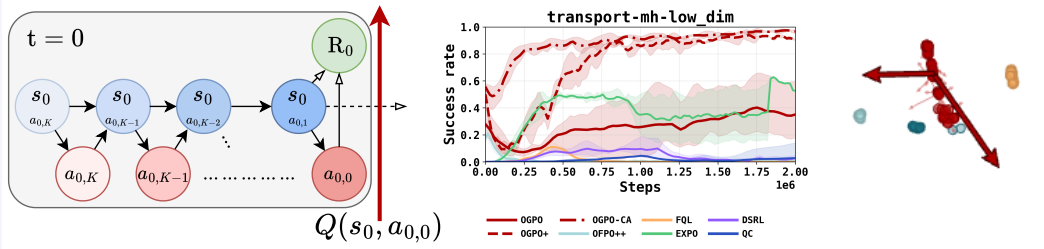


Figure 1: OGPO enables sample-efficient full-policy finetuning of generative control policies. **Left:** A GCP induces a denoising MDP inside each environment step. **OGPO** severs the bi-level MDP at the executed action and uses an off-policy critic as a terminal reward for PPO-style optimization over purely computational denoising trajectories. **Middle:** This off-policy policy extraction substantially improves sample efficiency on challenging manipulation tasks compared to prior GCP finetuning methods. **Right:** Unlike steering, residual learning, or behavior-cloning extraction, **OGPO** updates the full generative process using both positive and negative advantage gradients computed via Q-functions, allowing the policy to move toward high-value actions while clustering around multiple high success modes.

^a{sarveshp, mananaga, ssaxena2, dchen3, chaoyip, naichieh, giria, msimchow}@andrew.cmu.edu

^b{nakamoto, svlevine}@eecs.berkeley.edu

^c{jessezha, cleahw, abhgupta}@cs.washington.edu

^d{hongkai.dai, paarth.shaah}@tri.global

Code: TBD

Abstract

Generative control policies (GCPs), such as diffusion- and flow-based control policies, have emerged as effective parameterizations for robot learning. This work introduces Off-policy Generative Policy Optimization (**OGPO**), a sample-efficient algorithm for finetuning GCPs that maintains off-policy critic networks to maximize data reuse and propagate policy gradients through the full generative process of the policy via a modified PPO objective, using critics as the terminal reward. **OGPO** achieves state-of-the-art performance on manipulation tasks spanning multi-task settings, high-precision insertion, and dexterous control. To our knowledge, it is also the only method that can *fine-tune poorly-initialized behavior cloning policies to near full task-success with no expert data in the online replay buffer*, and does so with *few task-specific hyperparameter tuning*. Through extensive empirical investigations, we demonstrate the **OGPO** drastically outperforms methods alternatives on policy steering and learning residual corrections, and identify the key mechanisms behind its performance.

1 Introduction

Autonomous acquisition of new skills is an important challenge for modern robot manipulation. While imitation learning via behavior cloning (BC) from human demonstration can enable a robot to learn behaviors across several contexts, performance is typically brittle to subtle changes in tasks and environments. These models rarely exhibit high success rates zero-shot in the diversity of settings encountered in deployment. While this fragility can be remedied through additional data collection, a natural question to ask is - can the robustness of pre-trained imitation learning policies be bolstered autonomously without requiring considerably more manual data collection?

To this end, there has been a strong interest in finetuning pre-trained robotic policies via reinforcement learning (RL), to autonomously improve behavior via self-collected experience. Of particular relevance is the problem of finetuning *Generative Control Policies* (GCPs) - the parametrization of control policies by expressive generative models, such as diffusion or flow models [Chi et al., 2023, Black et al., 2024, Pan et al., 2025]. These policies have been extremely effective for modern robotic applications [Zhang and Gienger, 2024, Wolf et al., 2025].

Current methodology for GCP finetuning succumbs to tradeoffs between data efficiency and the extent of policy improvement during training. Approaches focused on sample efficiency combine *off-policy* critic learning, enabling strong experience reuse, with either targeted *partial* finetuning of the GCP such as steering the initial generation noise or learning residual corrections, or instead use behavior cloning to imitate high-return actions. These approaches learn quickly when the base policy has strong coverage of optimal actions, but struggle with exploring new behavior. On the other hand, methods focused on eliciting maximum final task performance [Lei et al., 2025, Ren et al., 2024, McAllister et al., 2025] use *on-policy* policy gradient updates, which drive aggressive policy improvement at the expense of significantly compromised sample efficiency.

In this work, we propose a new algorithm - **OGPO** for full-finetuning of expressive GCPs, providing both sample-efficient and expressive policy updates via data-efficient off-policy reinforcement learning. Following [Ren et al., 2024, Black et al., 2023] **OGPO** views GCP optimization as a bi-level MDP, with a nested inner denoising MDP over the action generation steps of a GCP, and an outer environment dynamics MDP over actions actually executed in the environment. Importantly, in real-robotics tasks, collecting trajectories from the environment MDP is expensive, while generating action trajectories through the denoising MDP is purely computational and therefore cheap.

While direct policy optimization in the unrolled bi-level MDP can be very (environment-)sample inefficient [Ren et al., 2024, Zhang et al., 2025b], **OGPO** leverages the asymmetry of sample costs to perform decoupled policy optimization. **OGPO** performs sample-efficient off-policy Temporal Difference (TD)-learning to learn a Q function in the environment dynamics MDP over *expensive* environment samples, while using data-inefficient, but stable on-policy RL updates to extract policies from the inner denoising MDP over *cheap* GCP samples. Doing so allows for an off-policy policy optimization algorithm that is data-efficient (due to TD-learning in the environment dynamics MDP), while being expressive (due to on-policy RL finetuning in the denoising MDP)

Through careful empirical study, we show that **OGPO** is able to achieve both stable and expressive updates for finetuning GCPs in challenging robotics tasks. Based on empirical analysis of the shortcomings, we further propose **OGPO+**, an empirically optimized variant that incorporates improvements in test-time optimization such as Best-of-N planning via Q-functions and policy distillation from successful trajectories obtained via online RL. These improvements allow **OGPO+** to achieve state-of-the-art performance on a set of contact-rich simulation environments with varying horizons, degrees of freedom, and precision requirements, while requiring minimal hyperparameter tuning. Surprisingly, we show that **OGPO+** is able to fine-tune policies with *zero expert data* in the policy replay buffer. This is a fundamentally new capability that points towards the future possibility of finetuning models with minimal human data collected in a task-specific manner on deployment. We perform a careful set of analyses

to understand the impact of the decoupled optimization central to **OGPO**, and the impact of the design decision made in **OGPO+** - showing the efficacy of full-policy finetuning of GCPs under the right design choices.

2 Preliminaries

We formulate our algorithm as a *Markov Decision Process* (MDP) $M_{\text{ENV}} := (S, A, P_0, P, R, \gamma)$, with states $s \in S$, actions $a \in A$, initial state distribution P_0 , transition probabilities P , reward R , and discount factor $\gamma \in (0, 1)$. At each timestep t , the agent (e.g., robot) observes the state $s_t \in S$, takes an action $a_t \sim \pi(a_t | s_t) \in A$, transitions to the next state s_{t+1} according to $s_{t+1} \sim P(s_{t+1} | s_t, a_t)$ while receiving a reward $R(s_t, a_t)$.¹ For the MDP M_{ENV} , we let \mathbb{E}^π (resp. \mathbb{P}^π) denote the expectation (resp. probability distribution) over trajectories $(s_0, a_0, \dots, s_T, a_T)$ with length $T + 1$, with initial state distribution $s_0 \sim P_0$ and transition operator P . We train a policy to optimize the cumulative discounted return $J(\pi_\theta) = \mathbb{E}^{\pi_\theta} \left[\sum_{t \geq 0} \gamma^t R(s_t, a_t) \right]$. We also recall the Q-function

$$Q^\pi(s, a) := \mathbb{E}^\pi \left[\sum_{t \geq 0} \gamma^t R(s_t, a_t) \mid (s_t, a_t) = (s, a) \right] \quad (2.1)$$

and value function $V^\pi(s) := \mathbb{E}_{a \sim \pi(s)} [Q^\pi(s, a)]$. We apply action chunking [Zhao et al., 2023], where sequences of actions $a_{t:t+h-1}$ are predicted and executed in open-loop. For simplicity, we treat each action chunk as a single action in M_{ENV} , thereby preserving to the standard MDP notation. Thus, for the rest of the paper, a_t **refers to an entire action-chunk**, and rewards are adjusted appropriately (see Appendix A.1).

On-Policy Policy Gradient Methods. *Policy gradient* (PG) methods (e.g., REINFORCE [Williams, 1992]) improve policy performance by approximating the gradient of this objective w.r.t. the policy parameters:

$$\nabla_\theta J(\pi_\theta) = \mathbb{E}^{\pi_\theta} \left[\sum_{t \geq 0} \nabla_\theta \log \pi_\theta(a_t | s_t) r_t(s_t, a_t) \right], \quad (2.2)$$

where $r_t(s_t, a_t) := \sum_{\tau \geq t} \gamma^\tau R(s_\tau, a_\tau)$ is the discounted future return from time t , and $\nabla_\theta \log \pi_\theta(a_t | s_t)$ denotes the gradient of the logarithm of the *likelihood* of $(a_t | s_t)$. Myriad improvements exist to reduce variance of gradient estimation and accelerate training stability; following [Ren et al., 2024, Zhang et al., 2025b], we build on the PPO algorithm [Schulman et al., 2017]. PG methods are called *on-policy* because they optimize over the *current* policy distribution, limiting data re-use and sample efficiency.

Off-Policy Reinforcement Learning. *Off-policy RL methods* maintain a long horizon replay buffer $\mathcal{D}_{\text{roll}} = \{(s_t, a_t, s_{t+1}, r_t, d_t)\}$ consisting of past states s_t , actions a_t , subsequent states s_{t+1} from the environment transitions, the observed rewards r_t , and the done signal d_t . The buffer is used to train an ensemble of M critic networks $Q_{\phi_i} : S \times A \rightarrow \mathbb{R}$, with parameters ϕ_1, \dots, ϕ_M , such that $Q_{\phi_i}(s_t, a_t)$ evaluates the expected cumulative return $Q^{\pi_{\bar{\theta}}}(s_t, a_t)$ of action a_t at state s_t under a current *target policy* $\pi_{\bar{\theta}}$. The critic networks are updated in parallel using the temporal difference loss, which enforces the Bellman consistency equation defined by Q-functions:

$$L_{\text{critic}}(\phi) = \mathbb{E} \left[Q_\phi(s_t, a_t) - \left(r_t + \gamma \cdot Q_{\text{targ}}(s_{t+1}, a_{t+1}) \right) \right]^2, \quad (2.3)$$

¹In practice, algorithms may be given incomplete or redundant state observation (e.g., via pixel measurements), in which case we can replace s with an observation o . This may violate the Markovian condition in the MDP, but still leads to well-posed algorithms.

where above the expectation \mathbb{E} is taken over $(s_t, a_t, r_t, s_{t+1} \sim \mathcal{B})$ sampled from the replay buffer \mathcal{B} , and each a_{t+1} is sampled independently from the current target policy $\pi_{\bar{\theta}}(\cdot | s_{t+1})$. To avoid overestimation bias, we set $Q_{\text{targ}}(s, a) = \frac{1}{M} \sum_i Q_i$ to be a mean over critic networks, described in the Appendix (Appendix A.1). [Fujimoto et al., 2018, Chen et al., 2021]. Importantly, (2.3) enables data collected by policies from previous training epochs, thereby increasing sample efficiency.

Generative Control Policies. Current robotic control policies use generative models as parameterizations of control policies. Following [Pan et al., 2025], we call these generative control policies (GCPs). GCPs represent a stochastic policy $\pi_{\theta}(\cdot | s)$ as a series of iterative computation steps, defined by a mapping $\bar{\pi}_{\theta} : S \times A \times \mathbb{N}$. Given a state s_t , the policy first samples $a_{t,K} \sim \bar{\pi}_{\theta}(\cdot | a_{t,k} = \emptyset, k = K, s_t)$ where k is a GCP timestep. Next, we sample $a_{t,k-1} \sim \bar{\pi}_{\theta}(\cdot | a_{t,k}, k, s_t)$ which leads to is an action $a_{t,0}$. We compactly denote the distribution of this action given the observation as $a_{t,0} \sim \pi_{\theta}(\cdot | s_t)$, turning the GCP into a standard policy. Our iteration conventions are *decreasing* in K , those in diffusion models. Following the same conventions, we also refer to the index k as the “denoising step.”

Flow-Based GCPs. We focus on a popular class of GCPs: flow-based control policies [Black et al., 2024]. As discussed in Appendix C, our methods and baselines can also be instantiated with Diffusion-based policies [Chi et al., 2023] and other controller parameterizations [Pertsch et al., 2025, Frans et al., 2024, Pan et al., 2025]. Flow policies are pretrained using the flow-matching objective: given training pairs (s, a) , we sample noise $z \sim N(0, \mathbf{I})$. With a continuous noise index $\tau \in [0, 1]$, we define an interpolated action $a_{(\tau)} = \tau + (1 - \tau)z$, and optimize a velocity field $v_{\theta}(a_{(\tau)}, \tau; s)$ by minimizing $\mathbb{E}_{(s,a,\tau)} \|v_{\theta}(a_{(\tau)}, \tau; s) - (a - z)\|^2$ [Albergo et al., 2023, Lipman et al., 2022]. Inference is performed by discretizing an ordinary differential equation (ODE) which reverses the noising process $a_{t,k-1} := a_{t,k} + \frac{1}{K} v_{\theta}(a_{t,k}, k/K, s)$, with $a_{t,0} \sim N(0, \mathbf{I})$.

3 Off-Policy Generative Policy Optimization

We propose Off-Policy Generative Policy Optimization, **OGPO**, an off-policy full-policy finetuning method for generative control policies. We begin by introducing the basic algorithm, and then describe an improved variant, **OGPO+**. We provide summary pseudocode in Algorithm 1, and defer full implementation details to Appendix B.

Background: Off-Policy Policy Extraction. Given a replay buffer $\mathcal{B} = \{(s, a, s', r)\}$, traditional off-policy RL methods consist of two steps: (1) fitting Q- functions via a TD-update Eq. (2.3), (2) performing policy extraction by choosing actions that maximize the target Q function Q_{targ} as a surrogate of future return:

$$\theta \in \arg \max_{\theta} \mathbb{E}_{a \sim \pi_{\theta}(s)} (Q_{\text{targ}}(s, a)). \quad (3.1)$$

The replay buffer facilitates off-policy data-reuse for training Q_{targ} (typically via (2.3)), driving sample efficiency, whereas (3.1) can be computed purely computationally. A historically popular approach to optimize this objective for simple policy parametrization, like Gaussian policies, is the so-called *reparameterization trick* [Kingma and Welling, 2013, Figurnov et al., 2018], where a stochastic policy is rendered as $\pi_{\theta}(s; w)$ for a noise w drawn from a fixed (non-learned) distribution. From here, Eq. (3.1) is written as an expectation over w , the algorithm directly differentiates $Q_{\text{targ}}(s, \pi_{\theta}(s, w))$ with respect to θ under samples w . In principle, the same can be done for GCPs such as flow-policies, sampling an initial noise $a_{t,K}$ and backpropagating through the inference chain (Figure 4, center). However, as

we show experimentally (Appendix H.1), doing so leads to an exploding gradient problem as we differentiate through the multiple flow steps. Moreover, it requires differentiating $\nabla_a Q_{\text{targ}}$, which can be inaccurate in contact-rich tasks [Suh et al., 2022].

OGPO: On-Policy PPO for Off-Policy Policy Extraction. OGPO is designed for applications, such as robotic manipulation, where environment interactions are more costly than computation, and where action gradients with respect to Q_{targ} are noisy or inaccurate [Suh et al., 2022]. We maintain off-policy critic learning that facilitates data reuse, and propose a *fully parallelizable zero-order optimizer* that solves Eq. (3.1), avoiding backpropagation through the denoising chain and differentiation with respect to the target network.

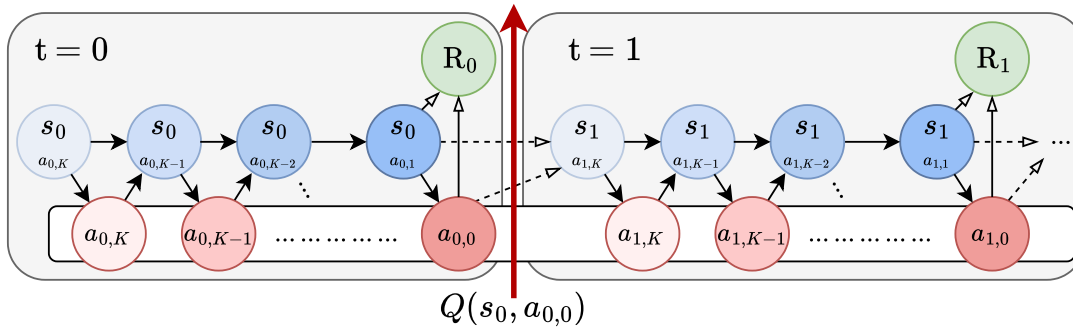


Figure 2: We recall the bi-level MDP from [Ren et al., 2024], which embeds action-level trajectories into the environmental dynamics. OGPO truncates this MDP at the end of each denoising trajectory, using Q-values as a terminal, action-trajectory-level reward. This enables off-policy policy extraction via on-policy policy optimization.

Our starting point is the bi-level MDP formulation adopted from [Ren et al., 2024] (Figure 2). Following [Black et al., 2023], we view sequences $a_{t,K:0} = (a_{t,K}, \dots, a_{t,0})$ as trajectories in an *denoising* MDP, where time is indexed by denoising step k , and state and action at step k are $a_{t,k}$ and $a_{t,k-1}$, respectively. Ren et al. [2024] embeds this action-level MDP into the environment-level MDP M_{ENV} , resulting in an *bi-level* MDP where states are $\bar{s}_{t,k} = (s_t, a_{t,k})$, the actions are $a_{t,k-1}$, and the indices (t, k) are lexicographically increasing in t and decreasing in k . Figure 2 depicts this bi-level MDP: transitions within each gray block occur within the denoising-level MDP, and between gray blocks are transitions in M_{ENV} ; see Appendix D for further details. The DPPO algorithm proposed by [Ren et al., 2024] then applies on-policy PPO at the level of this bi-level MDP. Whilst avoiding the aforementioned pathologies associated with backpropagation, this method gives up the sample efficiency afforded by off-policy critic learning.

Our **key insight** is that denoising-trajectories can be generated purely *computationally* from policy inference, as they occur in the “imagination” of the GCP. We can then use critic learning to sever the bi-level MDP just before environment-MDP state transitions (red line, Figure 2), enabling zero-order optimization applied only to the denoising-level MDP. As compared to backpropagation approaches to solving Eq. (3.1), our approach avoids (i) backpropagation through time and (ii) differentiating through the Q-function. Moreover, as compared to pure on-policy zero order optimization through the bi-level MDP [Ren et al., 2024], our zero-order updates are (i) performed purely computationally, in the “imagination” of the denoising process (ii) fully parallelized across large batch sizes (iii) used to optimize a critic network, facilitating full reuse of environment-level trajectories. Moreover, (iv) the problem horizon of the denoising-level MDP scales only with the denoising steps K , and not $K \times$ (task horizon). Concretely, we apply the PPO algorithm [Schulman et al., 2017], a zero-order policy gradient method, to optimize over the denoising MDP. Given state s_t , denoising trajectory $a_{t,K:0}$, and baseline value estimate

\hat{V} , we apply the standard PPO loss *only* to the denoising trajectory $a_{t,K:0}$:

$$\begin{aligned} \ell_{\text{PPO}}(\theta; s_t, a_{t,K:0}, \hat{\mu}) &:= \min(\omega_{\theta} \hat{A}, \text{clip}(\omega_{\theta}, 1 - \epsilon, 1 + \epsilon) \hat{A}) \\ \omega_{\theta} &:= \prod_{k=1}^K \frac{\pi_{\theta}(a_{t,k-1} | s_t, a_{t,k})}{\pi_{\hat{\theta}}(a_{t,k-1} | s_t, a_{t,k})}, \quad \hat{A} = Q_{\text{targ}}(s_t, a_{t,0}) - \hat{V}. \end{aligned} \quad (3.2)$$

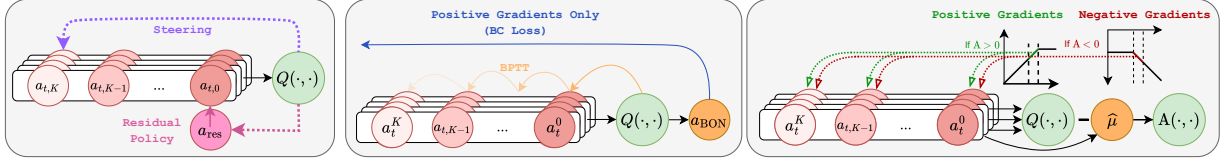


Figure 3: Visual depiction of the different off-policy RL algorithms. **(left)** DSRL trains an initial noise steering policy, while EXPO trains a residual policy to modify the final GCP action. **(center)** QC drives policy improvement via supervised finetuning (SFT) of Best-of-N actions ranked via the critic, while BPTT backpropagates the gradients sequentially through the entire GCP **(right)** OGPO uses an ensemble of critics to compute \hat{A}^G (Eq. (3.2)) that update the GCP via Annealed Importance Sampling, thereby directly conditioning the log-likelihoods over the GCP chain.

Multiple Denoising-Trajectory Sampling. Because denoising-trajectories are generated computationally, they can be resampled *fully in parallel* from *any* given state s_t in the replay buffer. Moreover, Q_{targ} can be evaluated without taking a single transition step in the environment. Taking advantage of this, we evaluate our PPO loss over an average of a batch of parallel-sampled trajectories, purely in the “imagination” of the GCP. By analogy to policy optimization in large language models (LLMs), we can think of a state s_t in the buffer as a “context” and the denoising trajectory $a_{t,K:0}$ as a “response”. We draw inspiration from the GRPO algorithm [Shao et al., 2024] in LLM post-training, where multiple responses are sampled in parallel from a given prompt, and gradients are averaged together to reduce gradient variance.² In OGPO, at each update, we sample N_{batch} states $(s^{(i)})_{1 \leq i \leq N_{\text{batch}}}$ from our replay buffer, and sample N_{group} denoising trajectories $(a_{K:0}^{(i,j)})_{1 \leq j \leq N_{\text{group}}}$ drawn i.i.d. from $\pi_{\hat{\theta}}(\cdot | s^{(i)})$ per state. We then update via the loss

$$\hat{L}_{\text{PPO}}(\theta) = \frac{1}{N_{\text{tot}}} \sum_i \sum_j \ell_{\text{PPO}}(\theta; s^{(i)}, a_{K:0}^{(i,j)}, \hat{V}^{(i)}). \quad (3.3)$$

Eq. (3.3) averages both over the states $s_t^{(i)}$ from the buffer (“prompts”), and denoising-trajectories generated in parallel from each given state (“responses”). This yields a normalization factor of $N_{\text{tot}} := N_{\text{batch}} \cdot N_{\text{group}}$. Moreover, parallel sampling facilitates estimating the value baseline via a direct Monte-Carlo approximation $\hat{V}^{(i)} \leftarrow \frac{1}{N_{\text{group}}} \sum_j Q_{\text{targ}}(s^{(i)}, a_0^{(i,j)})$, obviating the need to learn a separate value-prediction network.

Debiasing Noise Injection for Flow Policies. We instantiate OGPO for flow-based policies. To evaluate the likelihood ω_{θ} in Eq. (3.2), we must ensure the denoising-level action likelihoods $a_{k-1,t} | a_k, s_t$ are non-singular. ReinFlow [Zhang et al., 2025b] modifies the bi-level PPO algorithm of [Ren et al., 2024] for flow-based policies, achieving this by adding additional Gaussian noise to each flow step. For given choice of noise levels σ_k^2 , this yields the following inference procedure:

$$a_{k-1} \sim \tilde{\pi}^{\text{FLOW}}(\cdot | a_k, k, s) := N(v_{\theta}(a_k, \frac{k}{K}, s), \sigma_k^2 \mathbf{I}) \quad (3.4)$$

²GRPO includes an additional variance normalization term, which we omit.

In **OGPO**, we observe that naively adding noise can degrade policy performance by changing the marginal distributions of actions $a_{t,k}$ generated during denoising (Figure 21). We therefore introduce a correction proposed by Albergo et al. [2023] which (in the infinite step limit) ensures the per-denoising-step marginal distributions of noise-augmented actions match those of standard flow sampling; see also Liu et al. [2025]. See Appendix E.3 for details.

Algorithm 1 OGPO (Abbreviated)

```

1: for each environment step until done do
2:   Execute  $a_t \sim \pi_{\bar{\theta}}(\cdot | s_t)$ , and update buffer  $\mathcal{B} \leftarrow (s_t, a_t, r_t, s_{t+1}, \text{done})$ .
   % Standard Critic Update
3:   Update critic networks  $\phi_1, \dots, \phi_M$  using empirical TD Error (2.3) over  $\mathcal{B} \sim \mathcal{D}_{\text{roll}}$ .
   % Actor Update via Multiple Denoising Trajectories
4:   for  $i = 1, \dots, N_{\text{batch}}$  do
5:     Sample state  $s^{(i)}$  from  $\mathcal{B}$ , and action trajectories  $a_{k:0}^{(i,j)} \sim \pi_{\bar{\theta}}(\cdot | s^{(i)})$  for  $1 \leq j \leq N_{\text{group}}$ .
6:     Estimate value baselines via  $\hat{V}^{(i)} \leftarrow \frac{1}{N_{\text{group}}} \sum_j Q_{\text{targ}}(s^{(i)}, a_0^{(i,j)})$ 
7:   end for
8:   Update actor using aggregated PPO loss (3.3)
   % EMA parameters
9:   Update target parameters  $\bar{\theta} \leftarrow (1 - \tau)\bar{\theta} + \tau\theta$ ,  $\bar{\phi}_i \leftarrow (1 - \tau)\bar{\phi}_i + \tau\phi_i$ . Set  $Q_{\text{targ}} = \frac{1}{N} \sum_i Q_{\bar{\phi}_i}$ .
10: end for

```

OGPO: Core Insights

- **Off-Policy Q-learning for On-Policy GCP Extraction.** **OGPO** severs the bi-level MDP at environment transitions, using Q_{targ} as a terminal reward for the GCP’s denoising MDP.
- **0th-order optimization.** PPO-style zeroth order optimization over denoising trajectories avoids first order backpropagation through Q_{targ} and the GCP chain. This simplifies RL-finetuning in high-Lipschitz tasks.
- **Debiased noise injection.** SDE-augmented flow steps yield non-singular likelihoods for the PPO ratio ω_{θ} , with the stochastic interpolant correction ensuring marginal distributions match standard ODE inference. All $N_{\text{batch}} \times N_{\text{group}}$ trajectories are sampled and scored in parallel.

4 Improving **OGPO** by Mitigating Critic Over-exploitation

In this section, we identify a major limitation of **OGPO**: over-exploitation of learned critics due to highly expressive policy updates (Section 4.1). We then introduce three modular modifications to **OGPO** which overcomes this tendency, and which are mutually compatible:

- **OGPO+** (Section 4.2), which combines **OGPO** with behavior cloning regularization on *success-only* trajectories
- **OGPO+CA** (Section 4.3), which uses a *conservative advantage* for policy extraction, thereby *drastically mitigating the “dip” in offline-to-online adaptation*
- **OGPO+ χ^2** (Section 4.4), which adds in an additional χ^2 regularization term to a slowly-updated policy, and mitigates critic over-exploitation on pixel-based domains.

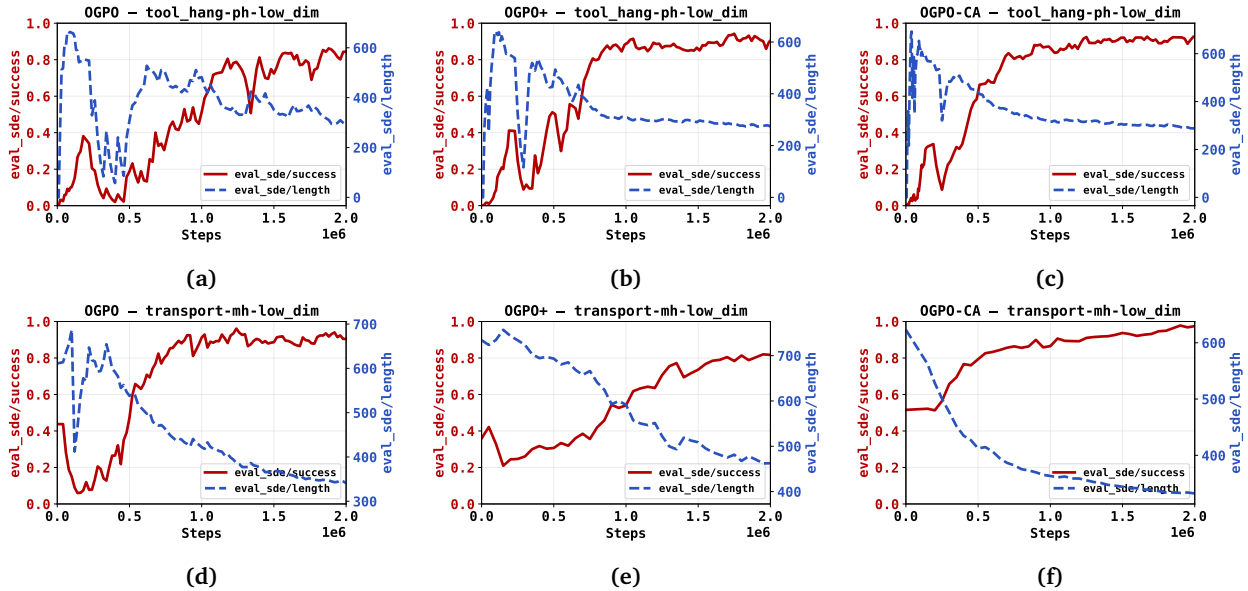


Figure 4: The above plots show the full training comparison between (a) Vanilla **OGPO**, (b) **OGPO+**, and (c) **OGPO+CA**, on state-based ROBOMIMIC tasks. The red axis shows success rate and the blue axis shows the mean length of *successful* trajectories. By aggressively maximizing sparse reward, **OGPO** optimizes for both task success rate, and *completion in few steps*. Without further regularization, the two can be in tension, causing a sharp initial decrease in the length of the policy rollouts, subsequent oscillations in success rates (TOOLHANG, (a) a high-precision task) or plateaus in performance (TRANSPORT, (d) a long-horizon task). By adding a success buffer, **OGPO+** biases the policy learning objective to favor task success (b, e). **OGPO+CA** mitigates the effect of outliers in the critic estimation, thereby fitting the “dip” between offline BC and online training (c, f).

For a practitioner, we recommend using **OGPO+CA** for state-based RL, and **OGPO+ χ^2** for pixel-based RL. In addition to these modifications, we optionally incorporate Q -variance reduction that averages the TD targets over N_{vr} actions sampled from the reference actor, thereby improve critic accuracy:

$$L_{critic,vr}(\phi) = \mathbb{E} \left[Q_\phi(s_t, a_t) - \left(r_t + \gamma \cdot \frac{1}{N_{vr}} \sum_{i=1}^{N_{vr}} Q_{\text{targ}}(s_{t+1}, a_{t+1}^{(i)}) \right) \right]^2, \quad a_{t+1}^{(i)} \stackrel{\text{i.i.d.}}{\sim} \pi_{\hat{\theta}}(\cdot | s_{t+1}). \quad (4.1)$$

We find that Eq. (4.1) always yields some improvement, but this benefit is most pronounced in pixel-based environments; it makes a marginal difference in state-based settings on pre-training from full data.

Experimental Setup: To identify improved design choices, we consider experiments on the state-based and image-based ROBOMIMIC tasks, which are described in greater detail in Section 5.1. For state-based runs, we use all state-information directly; for image based runs, we pass image observations using a frozen PaliGemma VLM backbone from the pre-trained $\pi 0.5$ VLA [Intelligence et al., 2025]. Further details are given in Appendix I.

4.1 Vanilla **OGPO** Over-exploits Imperfectly Learned Critics

Recall that **OGPO** makes PPO-style updates to the denoising MDP. The combination of the expressive generative policies and PPO updates on the full-denoising trajectory risks causing OGPO to over-optimize the critic, overfitting to advantages which are poorly estimated.

Success-Speed Tradeoff. The typical “sparse-reward” manipulation setting assigns reward of -1 each time step a task remains uncompleted. Thus, minimizing cumulative reward introduces a tension between completion *rate* and completion *speed*. As a result, **OGPO** may attempt to finish tasks too quickly, causing success rates to drop, harming future exploration training stability. This success-speed tradeoff is visible in Figure 4a, where we see average task length rapidly improves, but success rate plateaus. Anecdotally, we found that the variance-reduced critic update Eq. (4.1) did not improve this tradeoff.

Overexploitation is Exacerbated in Pixel-Based RL. We observe that vanilla **OGPO** has more severe exploitation in pixel-based settings. We consider a ROBOMIMIC SQUARE environment described above, where pixels are featurized using a frozen PaliGemma VLM backbone $\pi 0.5$. To isolate the effects of pixels, we compare four variants: (1) state-based actor/state-based critic; (2) pixel-based actor/state-based critic (3) pixel-based actor/pixel-based (4) state-based actor/pixel-based critic. We plot variants (1-3) in Figure 5, and omit (4) due to collapsing runs. We that the policy trains effectively for both state-based critic runs (1)&(2), but fails on (3)&(4), suggesting that *pixel-based* critics prevent learning. We hypothesize that such critics learn less accurately due to the richer observation space, making them more susceptible to exploitation via OGPO. Anecdotally, we found that the variance-reduced critic update made modest but very limited improvements to the pixel-based critics, suggesting the need for further interventions.

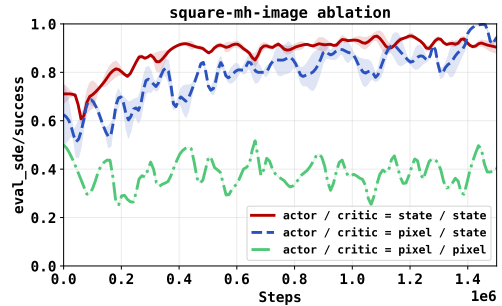


Figure 5: On ablating actor and critic observation modalities, we observe that vanilla **OGPO** fails to improve policy performance from image-based critics.

4.2 **OGPO+**: Regularizing **OGPO** With Behavior Cloning of Successful Trajectories

To remedy critic overexploitation, these challenges, **OGPO+** incorporates a regularization term applied only to actions from successful trajectories. This biases policy improvement toward replicating only the actions that led to success [Oh et al., 2018]. Specifically, we maintain a *success buffer* $\mathcal{D}_{\text{succ}} \subseteq \mathcal{D}_{\text{roll}}$ containing transitions from episodes that achieve task success. During training, we sample mini-batches from $\mathcal{D}_{\text{succ}}$ and compute

$$L_{\text{BC}}(\theta) = \mathbb{E}_{(s_t^{\text{succ}}, a_{t,0}^{\text{succ}}) \sim \mathcal{D}_{\text{succ}}} \left[\text{BCLoss}(\tilde{\pi}_{\theta}(\cdot | s_t^{\text{succ}}), a_{t,0}^{\text{succ}}) \right] \quad (4.2)$$

where BCLoss is the appropriate behavior cloning objective (e.g., denoising score matching for diffusion policies, or flow matching loss for flow policies). Success-imitations grounds the policy toward known good actions, while the PPO objective more aggressively explores improvements. For **OGPO+**, the total policy loss combines both terms:

$$L_{\text{Total}}(\theta) = L_{\text{PPO}}(\theta) + \lambda_{\text{BC}} L_{\text{BC}}(\theta). \quad (4.3)$$

(Optional) Best-of-N Inference. In many domains, such as language modeling, evaluating the quality of an action, or “verification” is learned more quickly and accurately than “generation” of good actions. This verification-generation gap [Setlur et al., 2025] motivates the popular practice of Best-of- N sampling [Brown et al., 2024], where one generates multiple proposal actions, and selects the best using a learned verifier.

Best-of- N sampling has seen widespread adoption in RL training of robotics policies

[Mark et al., 2024, Dong et al., 2025, Li et al., 2025], using the target critic as verifier. In, **OGPO+** we do the same with a slightly modified critic Q_{BoN} described in Appendix A.1. We remark that, due to the aggressive policy extraction, Best-of- N inference yields only **marginal additional** performance; the success buffer, as described above, is crucial. Thus, we recommend *omitting* Best-of- N when inference cost is constrained.

$$a_{\text{BoN},t} := \arg \max \{ Q_{\text{targ}}(s_t, a_{t,0}^{(i)}) : a_{t,0}^{(1)}, \dots, a_{t,0}^{(N)} \stackrel{\text{i.i.d.}}{\sim} \pi_{\theta_{\text{EMA}}}(\cdot | s_t) \}. \quad (4.4)$$

4.3 **OGPO+CA**: Mitigating the Offline-to-Online Performance Dip via Conservative Advantages

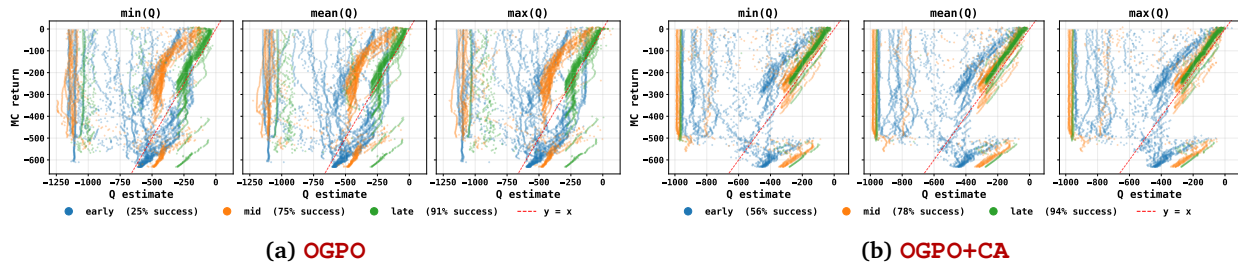


Figure 6: We perform a small sweep of ablations adding Best-of- N (BoN) Inference and Success Buffer on ROBOMIMICTOOLHANG.

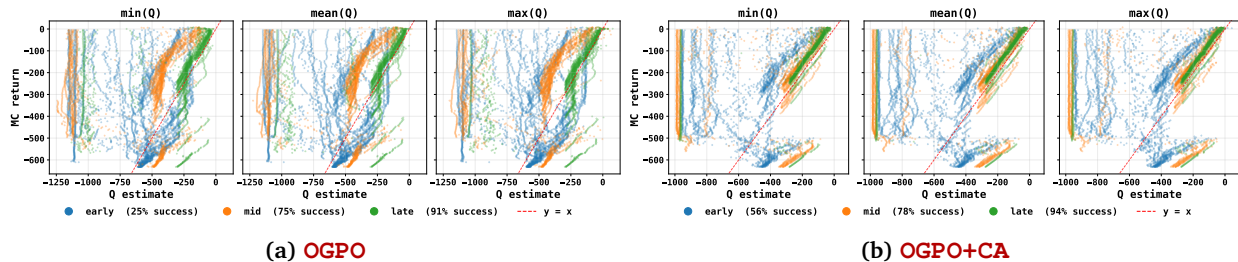


Figure 7: We take early-, mid-, and late- training checkpoints for **OGPO** and **OGPO+CA** to rollout 32 trajectories and visualize the min, mean, and max Q vs Monte-Carlo returns. (a) Shows **OGPO**’s Q values fluctuating widely between positive and negative values. (b) Shows **OGPO+CA**’s Q values converging more stably around the $y = x$ axis

A second challenge in offline-to-online RL is the pervasive “dip” in performance that arises transitioning from offline pretraining to online RL. Warm-starting methods like [Uchendu et al., 2023, Zhou et al., 2024] propose the use of high update-to-data (UTD) ratios and/or offline datasets during online RL, and the use of pessimistic critic updates. Anecdotally, we find that neither of these methods suffice. Moreover, from Figure 7a, we see that both over- and under-estimation of the Q values are possible, and both outliers potentially destabilize training. Thus, we instead to have the policy extraction step maximize the **conservative advantages**. This is made possible because our zero-order extraction takes advantages directly, and also accounts for the fact that global additive errors in critic values are less salient than incorrect *advantage* estimation.

For a given action a_i , we set

$$\hat{A}_i^{\text{cons}} = \begin{cases} \min_m A_{i,m} & \text{if } \min_m A_{i,m} > 0, \\ \max_m A_{i,m} & \text{if } \max_m A_{i,m} < 0, \\ 0 & \text{otherwise.} \end{cases} \quad (4.5)$$

where we recall $A_{i,m} = Q_{\phi_m}(s, a_i) - \frac{1}{N_{\text{group}}} \sum_{i'=1}^{N_{\text{group}}} Q_{\phi_m}(s, a_{i'})$ is the group-wise advantage using the m -th network in the ensemble. Eq. (4.5) provides a non-zero advantage (and thus updates the policy) if and only if *all* advantages have the same sign, thereby robustifying updates to estimation errors in the critic networks. As shown in Figure 7b, we see that policy extraction with conservative advantages also improves the calibration of critic estimation, in that critic values in earlier states of training more tightly track those in later stages.

4.4 **OGPO+ χ^2** : Overcoming critic exploitation on images via χ^2 regularization

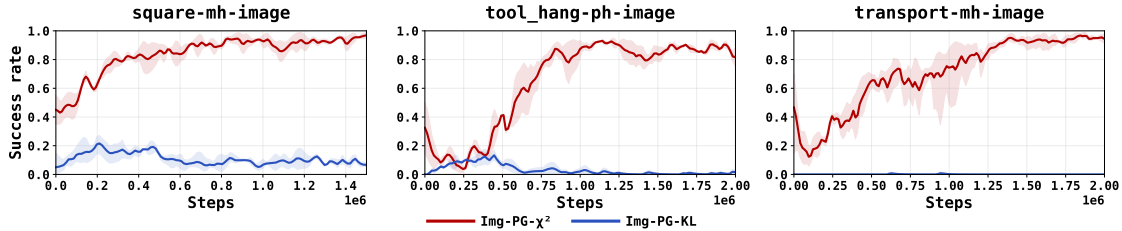


Figure 8: We

In principle, the PPO clipping mitigates serves as an approximation for a KL trust-region, which has the intended affect of regularizing the policy to mitigate critic over-exploitation. However, given that the generative policies in **OGPO** are more expressive than traditional monolithic RL policies, we find above that PPO clipping does not suffice. Instead, we leverage a stronger form of regularization - χ^2 regularization, motivated by its stronger coverage properties [Huang et al., 2024]. Concretely, we propose a regularized variant of **OGPO** we call **OGPO+ χ^2** . **OGPO+ χ^2** adopts the best practices of **OGPO+**, and additionally maintains a slow exponential moving average policy, denoted as π_{slow} (with update rate $\tau_{\text{slow}} \ll \tau$). We then replace the GRPO advantage in Eq. (3.2) with the drift-penalized variant

$$\hat{A}_{\chi}^{(i,j)} := \hat{A}^{(i,j)} - \beta \omega_{\theta, \text{slow}}, \quad (4.6)$$

where ω_{θ} is the ratio term from Eq. (3.2). In Appendix E.2, we demonstrate that maximizing Eq. (4.6) is mathematically equivalent to adding a regularization on the χ^2 difference between action-trajectories from π_{θ} and π_{slow} . In Appendix E.2, we verify that χ^2 regularization is *essential*, showing that other natural regularizers fail to ensure convergence on pixel-based tasks Figure 8.

5 When does Full-Finetuning (**OGPO**) Improve Over Popular Baselines?

In this section, we carefully compare **OGPO**, **OGPO+**, and **OGPO+CA** to a number of popular baselines to elucidate the merits and limits of its design philosophy— full policy fine-tuning, off-policy critic learning, and PPO policy extraction. Our experiment environments are representative of many common challenges in robot learning (e.g. high precision, long horizon, mixed data quality), and baselines cover competing design philosophies (e.g. steering, residual learning).

Criterion	OGPO	QC	DSRL	EXPO
Mixed Data Quality	✓✓	✓✓	✓✓	✗✗
High Precision Tasks	✓✓	✗✓	✗✗	✓✓
Partial Demonstrations	✓✓	✓✓	✗✓	✗✗
Long Horizon	✓✓	✓✗	✓✗	✗✗
Dense/Dexterous	✗✓	✗✓	✓✗	✓✓
High Sample Efficiency	✓✓	✗✗	✗✗	✓✗

Table 1: Left (resp. right) symbol indicates achieving high success With (resp. Without) task-specific hyperparameter tuning. ✗- fails to converge on all tasks; ✓- converges on some but not all tasks; ✗✓- converges on all tasks, but below SOTA success/efficiency; ✓✓- converges on all tasks, competitive with SOTA success/efficiency. We use the optimized variants where possible (e.g. **OGPO+** for **OGPO** and similarly for all the baselines).

Summary of Findings. We summarize comparisons to other off-policy methods in Table 1. Each method has two columns: left denotes if the method converges with task-optimized hyperparameters,

and right denotes fixed hyperparameters across all tasks within the criterion (see Appendix J). The markings are explained in the table caption.

We find that **OGPO** is able to learn in sparse-reward tasks with mixed/partial data quality and on high-precision/long horizon tasks, whereas other methods struggle in one or more of these regimes. It also exhibits (often times drastic) gains in sample efficiency compared to these methods, and order-of-magnitude improvements related to the on-policy **DPPO** algorithm. However, **OGPO** is less performant on the dense-reward tasks from the Adroit Hand benchmark (Figure 11).

Comparisons are detailed further in Section 5.2. Sample efficiency improvements v.s. **DPPO** are expected (off- vs. on-policy), and we attribute gains against off-policy baselines to exploration behavior and expressive policy updates, studied in Section 6.1. Appendix H ablates the merits of zero-order vs. backpropagation through time, the role of *negative-advantage gradients* in encouraging exploration, and the enhancements distinguishing **OGPO** and **OGPO+**.

5.1 Experimental Setup

Baselines. We compare against the baselines mentioned in Section 7.3, which are described in more detail in Appendix F. In short, we consider: (i) **DPPO** [Ren et al., 2024], representative of on-policy learning, (ii) **DSRL** [Wagenmaker et al., 2025], representative of off-policy noise steering (iii) **EXPO** [Dong et al., 2025], representative of learning residual corrections to the GCP, and (iv) to a variant of **QC** [Li et al., 2025] representative of behavior cloning policy extraction. We do not compare to ReinFlow [Zhang et al., 2025b] due to reported reduced sample efficiency compared to **DPPO**, making the latter a more compelling baseline. We also skip comparison to PA-RL [Mark et al., 2024] for reasons described in Appendix E.6. Lastly, we introduce a steering+residual learning baseline, (v) **S/R**, combining **DSRL** and **EXPO** to (hypothetically) yield the benefits of both. For a fair comparison with **OGPO+**, we implement each baseline with its own best-practices, as described in Appendix F.

Environments. Our simulation environments are chosen to elicit key challenges faced in modern robot learning: *Robomimic*: To test high-precision robotic control, we use three ROBOMIMIC tasks [Mandlekar et al., 2021]: SQUARE (medium-horizon insertion), TOOLHANG (long-horizon multi-step insertion), TRANSPORT (bi-manual long-horizon transfer). SQUARE and TRANSPORT use Multi-Human (MH) datasets; TOOLHANG uses Proficient-Human (PH) with BC stopped at 50% success. *Franka Kitchen*: We use the FRANKA-KITCHEN benchmark [Gupta et al., 2019] with a 9-DoF Franka robot manipulating 4 kitchen objects, testing sensitivity to multi-step trajectories with complete demonstrations (KITCHEN-COMPLETE), randomized subtask orders (KITCHEN-MIXED), and sequential partial trajectory data (KITCHEN-PARTIAL). *Adroit*: To test performance in dextrous manipulation tasks with dense-reward, we use the 24-DoF Adroit Hand benchmark: DOOR-V1, HAMMER-V1, PEN-V1, RELOCATE-V1 for door opening, hammering, pen reorientation, and object relocation. Expert datasets from D4RL/Minari. *LIBERO*: Finally, to test pixel-based language-conditioned manipulation, we use the LIBERO benchmark [Liu et al., 2023]. Further details are given in Appendix I.

Experimental Regime: Online RL from a BC Checkpoint. We emulate real-world robot learning settings where large-scale pretrained policies with varying levels of online success rates are deployed to learn novel tasks without access to large offline datasets. Thus, we pre-train a flow GCP for all baselines, clip it to at most 50% success rate, and use the same BC checkpoint for all baselines in online RL without additional data. Full details in Appendix J.1.

5.2 Comparison to other methods

Expressivity: Full-Policy Finetuning (OGPO) vs. Steering (DSRL) vs. Residual (EXPO). Next, we compare **OGPO** to performant off-policy alternatives that do not fine-tune the full GCP across 11 tasks. *Steering (DSRL)* can be sample-efficient but relies on sufficient base policy action coverage, leading to

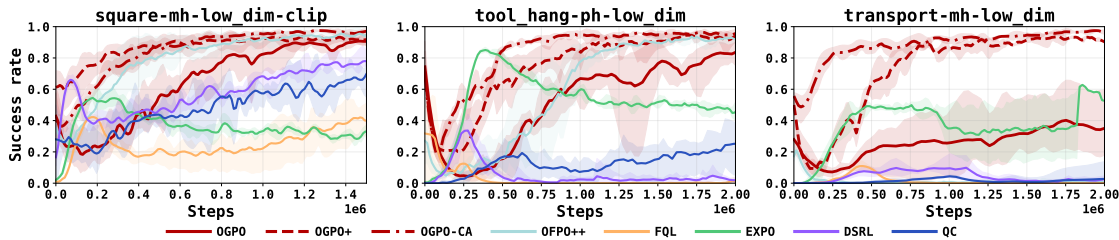


Figure 9: Comparison against natural off-policy baselines (EXPO, DSRL, QC), and on-policy algorithms modified to use OGPO-style off-policy advantages (OFPO++, FQL) on ROBOMIMIC SQUARE, TOOLHANG, and TRANSPORT.

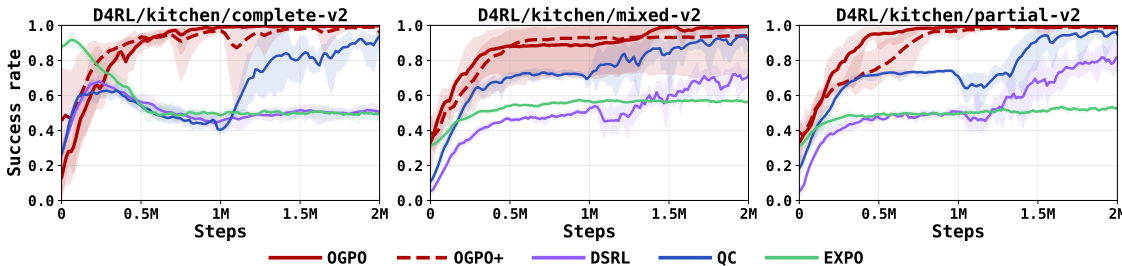


Figure 10: Comparison against natural off-policy baselines (EXPO, DSRL, QC) on FRANKA-KITCHEN

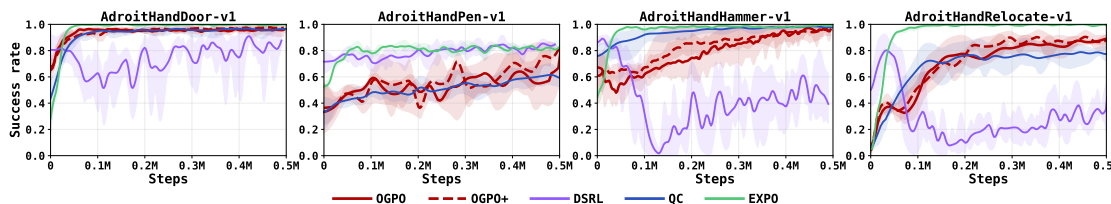


Figure 11: Comparison against natural off-policy baselines (EXPO, DSRL, QC) on the AdroitHand

suboptimal performance when the base policy’s performance is poor, such as in KITCHEN tasks. Further, by not updating later steps of the GCP, steering struggles on high-precision tasks such as the ADROIT task suite. We also empirically found it to be sensitive to hyperparameters; in some tasks, DSRL performance crashes despite heavy tuning. We attribute some of this instability to our use of DSRL on a flow-based GCP instead of a diffusion-based GCP; the original paper uses diffusion GCPs for low-data-coverage experiments. However, we are also more sample-efficient than DSRL’s paper-reported numbers on shared tasks.

Residual learning (EXPO) can perform well when the base policy is strong and thus only minor residual corrections are needed (it is highly performant in ADROIT in Figure 9), but, just like steering (DSRL), it generally performs poorly or is unstable when the base policy performance starts lower (KITCHEN and most ROBOMIMIC tasks). We note that when given offline data, EXPO can perform well (see Figure 18), but our experimental regime is without access to the pre-training data. Our Steering + Residual Learning (S/R) baseline combines EXPO and DSRL; we plot sample efficiency curves in ROBOMIMIC tasks in Figure 27, where we see that it is better than EXPO/DSRL alone in SQUARE, albeit still worse compared to OGPO, and demonstrates unstable training in the high precision TOOLHANG task.

Off-Policy Learning vs. Self-Distillation/Behavior Cloning (BC) with QC. Next, we compare policy extraction methods. We find the action-chunked BPTT variant proposed in the QC paper to perform poorly (Fig. 25) on flow policies, and thus use a variant that explores online with Best-of-N action sam-

pling and fine-tunes the BC policy on transitions from the online replay buffer. **QC** plateaus at lower performance for most tasks, requires more task-specific hyperparameter tuning, and has worse sample efficiency. We attribute this to SFT’s inability to expand the support of the GCP action distribution, required for sufficient exploration.

Off-Policy OGPO vs. On-Policy DPPO. We begin by comparing **OGPO+** against **DPPO**, where the major difference between the two is that **OGPO+** truncates the bi-level MDP proposed by **DPPO** at the end of each denoising trajectory with terminal rewards coming from an off-policy Q-function, while **DPPO** treats the entire bi-level MDP as a single MDP to train with on-policy RL. On final success rates across ROBOMIMIC SQUARE and TRANSPORT, this off-policy modification results in **DPPO** taking $\sim 10\times$ longer to reach the final success rates achieved by **OGPO+**. Overall, we find that both **OGPO** and **OGPO+** outperform **DPPO**’s paper-reported results in both sample efficiency and final performance across all shared tasks, even with matched network architectures and action chunk lengths.

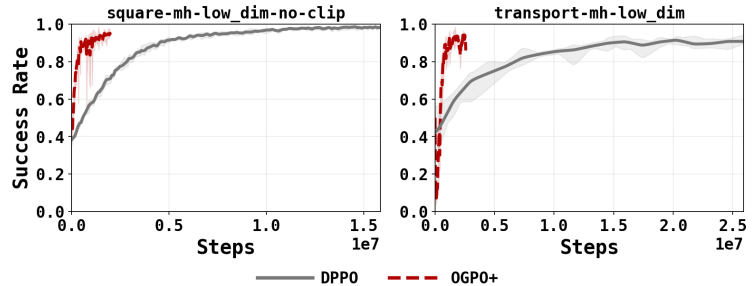


Figure 12: **OGPO+** substantially improves sample efficiency compared to the on-policy **DPPO** algorithm.

6 Understanding and Ablating The Merits of **OGPO**

6.1 Does **OGPO** Encourage Exploration?

As illustrated in Figure 14, policies trained via Behavior Cloning (BC) exhibit a *mode-seeking* behavior, agnostic of the underlying environment MDP and task rewards. This causes the BC policy to collapse variance rapidly to adhere to narrow "cone" of demonstrated trajectories. In contrast, **OGPO** leverages Q-functions to drive action distribution *manifold expansion* toward high-value regions beyond the support of the offline action distributions. During policy updates, we compute the annealed importance sampling ratio ω for the online policy π_θ with respect to the EMA policy $\bar{\pi}_\theta$ and weigh ω against the advantage (\hat{A}^G) to guide the entire GCP chain to explore actions that lead to high-value states via the Q-functions.

We demonstrate this exploration tendency by visualizing the action distributions for the different baselines on critical states obtained from TOOLHANG at the end of BC pretraining, and the Initial, Mid, and End stages of RL finetuning. Figure 13 shows a UMAP [McInnes et al., 2018] plot of the natural baselines compared with **OGPO+**

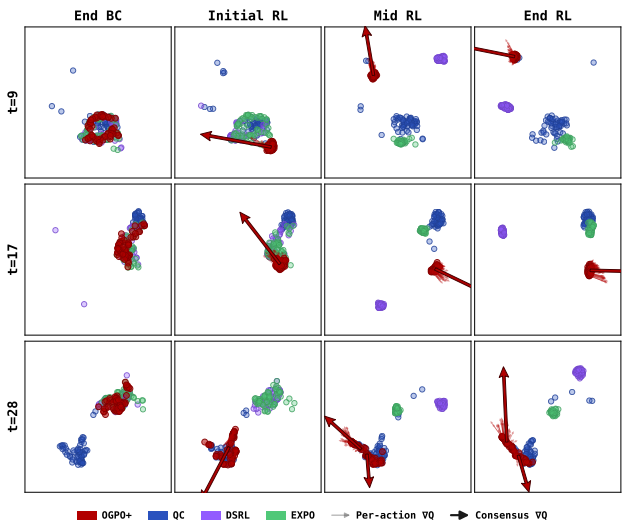


Figure 13: Actions generated by BC policies on critical states in TOOLHANG overlap in the UMAP space and diverge as training progresses. **OGPO** policies generate actions along narrower variance of successful actions compared to the baselines. We also see that $\nabla_a Q(s, a)$ nudges the actions away from this variance axis toward more efficient execution

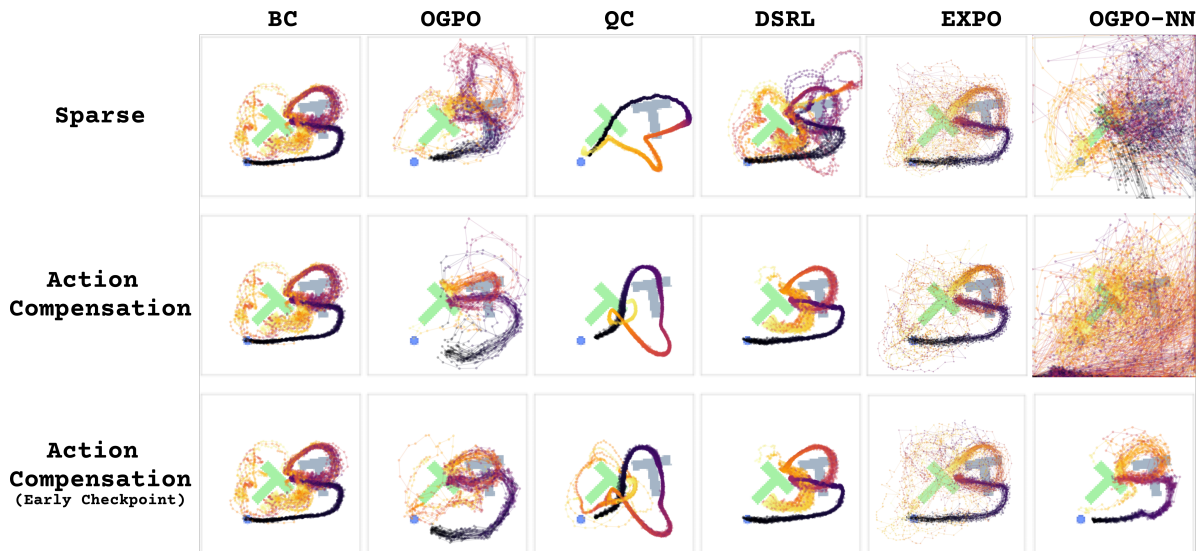


Figure 15: **OGPO** exhibits manifold expansion by making the policy more multimodal as well as execution efficient. We compare against the natural baselines and a no-negative gradient version of **OGPO**, in (top) sparse reward, (middle) sparse reward with Δa_t compensation, and (bottom) early-stage policy sparse reward with Δa_t compensation settings. We observe that **OGPO** policies in sparse reward settings optimize for execution speed along with task success.

and visualizes the $\nabla_a Q(s, a)$ vector pulling away from the action distribution in the UMAP space. We also visualize the differences in **OGPO**, **OGPO+**, and **OGPO+CA** in Figure 22 and note that **OGPO+CA** generates significantly stronger consensus $\nabla_a Q(s, a)$ values, especially in the initial stages of training which validates that conservative advantages result in a stronger alignment of the Q functions.

We empirically show the effects of **OGPO** along with all the baselines on a Push-T task from [Chi et al., 2023] and elucidate a detailed summary of the optimization and exploration behavior of **OGPO** in Appendix G.

6.2 Which Design Decisions Explain the Performance of **OGPO** and **OGPO+**?

In the interest of space, full ablation details are deferred to Appendix H; here, we summarize the main takeaways. First, zero-order PPO extraction is crucial: directly backpropagating through the denoising chain often fails catastrophically, supporting our choice to optimize the GCP through likelihood ratios rather than through $\nabla_a Q(s, a)$. Second, Best-of- N inference provides only marginal gains by itself and can increase oscillations when the critic is imperfect, whereas the success buffer in **OGPO+** consistently improves sample efficiency and asymptotic performance by anchoring policy improvement to successful behavior. Third, negative-advantage gradients are important on high-precision and long-horizon tasks, where merely imitating high-value samples is insufficient to suppress bad modes. Finally, we find that GRPO-style variance normalization hurts performance, pes-

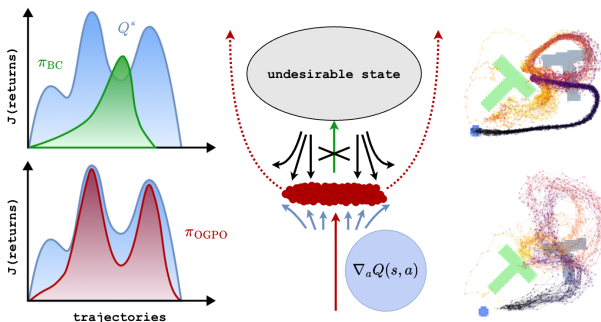


Figure 14: As needed by the task in question, generative control policies extracted via **OGPO** exhibit multimodality by faithfully aligning Q-functions toward Q^* .

simistic min-of-ensemble critics can be overly conservative during early online learning, and flow- and diffusion-based instantiations of **OGPO** perform comparably, suggesting that the main gains come from the extraction mechanism rather than the particular GCP parameterization.

6.3 Does PPO policy extraction outperform AWR and FPO extraction?

We next compare **OGPO**'s PPO-style policy extraction against a number of alternatives: (1) **AWR-FM** which combines advantage-weighted regression (AWR, [Peng et al., 2019]) to re-weight the flow-matching loss by exponentiated advantages; **AW-OGPO**, which uses exponentiated advantages as in Peng et al. [2019], but instead reweights the **OGPO** likelihood ratio consider in Eq. (3.2); and **OFPO++**, which performs policy extraction by using FPO++ [Yi et al., 2026] advantage on the noising MDP. Detailed descriptions of these strategies are given in Appendix H.5. In addition, we generally fine **AW-OGPO** to outperform **AWR-FM**, so we add a positive-only variant of **AW-OGPO** given as $\hat{A}^G \leftarrow \exp(\hat{A}^G/\beta) \cdot \mathbb{I}[A > 0]$. Otherwise, all these methods use the same replay data, critic training, and group-wise advantages.

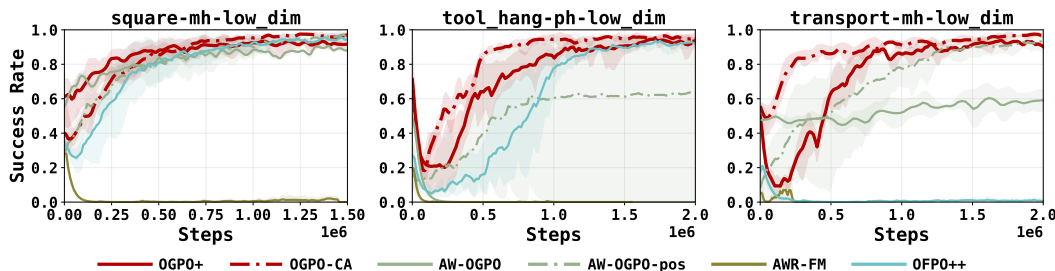


Figure 16: **OGPO** comparisons with policy extraction ablations with **AWR-FM**, **AW-OGPO** and **OFPO++** on ROBOMIMIC environments

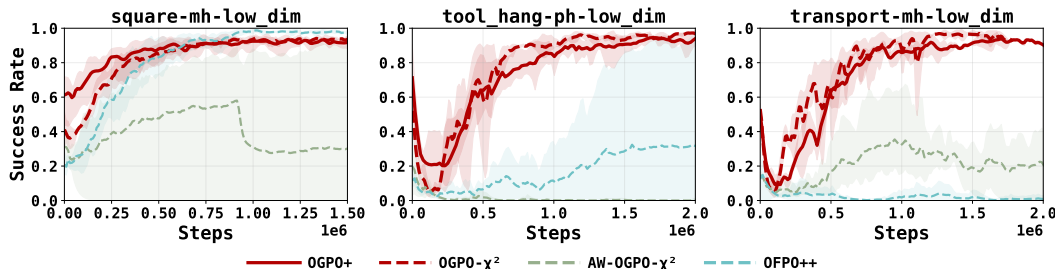


Figure 17: **OGPO** comparison with policy extraction ablations with **AWR-FM**, **AW-OGPO** and **OFPO++** on ROBOMIMIC environments

As shown in Figure 16, **AWR-FM** fails across the ROBOMIMIC tasks, indicating that pure advantage-weighted regression is not enough for finetuning expressive GCPs from imperfect critics. **AW-OGPO** improves over **AWR-FM**, and **OFPO++** is more competitive, but both remain less stable than clipped PPO extraction, especially on TOOLHANG and TRANSPORT. Adding χ^2 regularization deteriorates the performance of **AW-OGPO** and **OFPO++** (Figure 17), suggesting that compared to **OGPO**, these policy extraction methods do not aggressively optimize the Q-functions via the advantage estimate \hat{A}^G .

7 Related Work

We situate our work within the landscape of generative control policies, reinforcement learning for robotic control, and finetuning strategies for iterative generative models.

7.1 Generative Control Policies

The success of diffusion models in image generation [Ho et al., 2020, Song et al., 2020, Rombach et al., 2022] has inspired their adoption for robotic control. Diffusion Policy [Chi et al., 2023] demonstrated that denoising diffusion probabilistic models (DDPMs) can effectively parameterize visuomotor policies by iteratively denoising action sequences conditioned on observations. Flow-matching policies [Lipman et al., 2022, Liu et al., 2022] offer a more efficient alternative by learning velocity fields that transport noise to action distributions through ordinary differential equations (ODEs), achieving comparable performance with fewer integration steps.

Recent work has sought to improve the generative modeling capacity. Notably, shortcut models [Frans et al., 2024] condition on desired step sizes to enable few-step generation, while consistency models [Song et al., 2023] distill multi-step diffusion into single-step generation. Recently, [Pan et al., 2025] introduced Minimally Iterative Policies (MIP), demonstrating that two-step regression-based policies can match full flow model performance, suggesting that distributional learning may be less critical than previously believed. Orthogonally, tokenized autoregressive policies such as FAST [Pertsch et al., 2025] encode continuous action chunks via discrete cosine transforms to enable efficient training of vision-language-action (VLA) models on high-frequency control data.

For **OGPO**, we demonstrate flow and diffusion-based policies as representative of the general IGP formulation and leave generalization to other formulations as future work.

7.2 Reinforcement Learning for Robotic Policy Finetuning

The incorporation of Reinforcement Learning (RL) into robotic policy training mirrors the post-training paradigm in large language models [Ouyang et al., 2022, Shao et al., 2024]. On-policy methods such as REINFORCE [Williams, 1992] and PPO [Schulman et al., 2017] update policies using only data from the current policy iteration, ensuring stable but sample-inefficient learning. DPPO [Ren et al., 2024] extends PPO to diffusion policies by computing policy gradients through the denoising chain, while ReInflow [Zhang et al., 2025b] applies similar principles to flow-matching policies.

Off-policy algorithms promise greater sample efficiency by maintaining replay buffers of past experiences. Classical approaches such as SAC [Haarnoja et al., 2018], TD3 [Fujimoto et al., 2018], and REDQ [Chen et al., 2021] learn Q-functions from off-policy data to guide policy updates. Temporal difference learning mitigates the requirement of the policy to compute Monte Carlo return to the go. However, naive application to IGPs in the RL-finetuning regime can exhibit training instabilities due to large initial distributional shifts and value overestimation. To mitigate these, [Mark et al., 2024, Li et al., 2025] proposed using Q functions merely to rank stochastic policy actions and fine-tuning the policy using the Best-of-N actions. However, driving policy improvement via Q-function ranking can be inefficient as it requires exploration away from the mean values of the flow policy.

Concurrently, RL-100 [Lei et al., 2025] presents a comprehensive real-world RL framework built on diffusion policies, demonstrating deployment-grade success rates across eight manipulation tasks. RL-100 adopts the same bi-level MDP formulation and clipped PPO surrogate as DPPO, unifying imitation and reinforcement learning under a single objective across both offline and online stages, and additionally incorporates consistency distillation for high-frequency deployment. While RL-100 demonstrates impressive real-world reliability, its policy optimization remains fully on-policy, requiring iterative offline data expansion to achieve sample efficiency. **OGPO** instead decouples the bi-level MDP via off-policy critic learning, achieving comparable or superior sample efficiency in simulation without requiring multiple rounds of offline RL pre-training.

7.3 Finetuning Strategies for Iterative Generative Policies

Existing approaches to finetuning IGPs differ along the axis of *what* is optimized. Steering methods, exemplified by **DSRL** [Wagenmaker et al., 2025], optimize the distribution over initial noise a_K while freezing the pretrained denoising network. This constrains policy improvement within the support of the pretrained IGP distribution. Residual policy approaches such as **EXPO** [Dong et al., 2025] train an additional network π^{res} that modifies the final action $a_{\text{res}} = \pi^{\text{res}}(a_{t,0}, s_t)$, allowing mode shifts within the BC policy support but fails to facilitate discovery of new behaviors.

Policy-agnostic RL (PA-RL) [Mark et al., 2024] and Q-chunking (**QC**) [Li et al., 2025] employ Q-functions to rank behavior cloned policies with high-value actions or use $\nabla_a Q(s, a)$. In the image generation domain, Flow-GRPO [Liu et al., 2025] concurrently applied GRPO [Shao et al., 2024] to flow matching models for text-to-image alignment, sharing with **OGPO** the ODE-to-SDE conversion for injecting stochasticity into deterministic flow policies and the use of group-relative advantage estimation over parallel denoising trajectories. However, Flow-GRPO operates in the on-policy, bandit-like setting: rewards are terminal (image-level), the “environment” is a single-step generation with no dynamics, and advantages are estimated via group normalization of final rewards rather than learned Q-functions.

In contrast, **OGPO** addresses the multi-step robotic control setting, where off-policy TD-learning is essential for sample efficiency across long environment horizons, and the two-level MDP structure enables reuse of costly environment transitions while performing on-policy updates purely within the denoising MDP. However, in addition to zero-order optimization via Q functions, **OGPO** performs

8 Conclusion and Limitations

We introduce **OGPO**, an approach that combines the best of on-policy and off-policy methods for finetuning generative control policies (GCPs) and enjoys high success rates and sample efficiency across numerous tasks. However, **OGPO** still has drawbacks: the use of full-policy finetuning may be needlessly expressive, and therefore slow, when large amounts of expert-quality data are added to the replay buffer (Figure 18). Moreover, it is possible that PPO policy extraction can over-exploit the Q-function, leading to either training collapse and/or tensions between success rate and speed of completion. As limited evidence of this, we see small oscillations in policy performance that prevent **OGPO** from reaching exact 100% success rates.

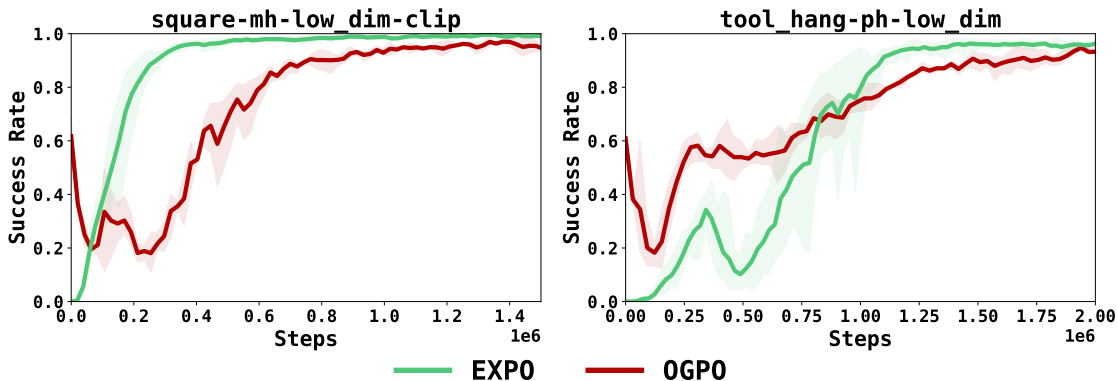


Figure 18: Comparison to EXPO with Offline-Ratio = 0.5

Acknowledgments

MN would like to thank Qiyang Li for helping with the initial implementation, and Seohong Park and Aviral Kumar for their informative discussions. This research used the Savio computational cluster resources provided by the Berkeley Research Computing program at UC Berkeley. MS would like to thank Aviral Kumar and Andrew Wagenmaker for useful discussions. SP would like to thank Steven Man, Andrea Bajcsy, and Ken Nakamura for insightful discussions. We acknowledge support from the Toyota Research Institute (TRI) University 2.0 program.

References

- Michael S Albergo, Nicholas M Boffi, and Eric Vanden-Eijnden. Stochastic interpolants: A unifying framework for flows and diffusions. *arXiv preprint arXiv:2303.08797*, 2023.
- Y. Bengio, P. Simard, and P. Frasconi. Learning long-term dependencies with gradient descent is difficult. *IEEE Transactions on Neural Networks*, 5(2):157–166, 1994. doi: 10.1109/72.279181.
- Kevin Black, Michael Janner, Yilun Du, Ilya Kostrikov, and Sergey Levine. Training diffusion models with reinforcement learning. *arXiv preprint arXiv:2305.13301*, 2023.
- Kevin Black, Noah Brown, Danny Driess, Adnan Esmail, Michael Equi, Chelsea Finn, Niccolo Fusai, Lachy Groom, Karol Hausman, Brian Ichter, et al. π_0 : A vision-language-action flow model for general robot control. *arXiv preprint arXiv:2410.24164*, 2024.
- Bradley Brown, Jordan Juravsky, Ryan Ehrlich, Ronald Clark, Quoc V Le, Christopher Ré, and Azalia Mirhoseini. Large language monkeys: Scaling inference compute with repeated sampling. *arXiv preprint arXiv:2407.21787*, 2024.
- Xinyue Chen, Che Wang, Zijian Zhou, and Keith Ross. Randomized ensembled double q-learning: Learning fast without a model. *arXiv preprint arXiv:2101.05982*, 2021.
- Cheng Chi, Siyuan Feng, Yilun Du, Zhenjia Xu, Eric Cousineau, Benjamin Burchfiel, and Shuran Song. Diffusion policy: Visuomotor policy learning via action diffusion. *arXiv preprint arXiv:2303.04137*, 2023.
- Perry Dong, Qiyang Li, Dorsa Sadigh, and Chelsea Finn. Expo: Stable reinforcement learning with expressive policies. *arXiv preprint arXiv:2507.07986*, 2025.
- Lasse Espeholt, Hubert Soyer, Remi Munos, Karen Simonyan, Volodymir Mnih, Tom Ward, Yotam Doron, Vlad Firoiu, Tim Harley, Iain Dunning, Shane Legg, and Koray Kavukcuoglu. Impala: Scalable distributed deep-rl with importance weighted actor-learner architectures, 2018. URL <https://arxiv.org/abs/1802.01561>.
- Mikhail Figurnov, Shakir Mohamed, and Andriy Mnih. Implicit reparameterization gradients. *Advances in neural information processing systems*, 31, 2018.
- Kevin Frans, Danijar Hafner, Sergey Levine, and Pieter Abbeel. One step diffusion via shortcut models. *arXiv preprint arXiv:2410.12557*, 2024.
- Justin Fu, Aviral Kumar, Ofir Nachum, George Tucker, and Sergey Levine. D4rl: Datasets for deep data-driven reinforcement learning. *arXiv preprint arXiv:2004.07219*, 2020.

- Scott Fujimoto, Herke Hoof, and David Meger. Addressing function approximation error in actor-critic methods. In *International conference on machine learning*, pages 1587–1596. PMLR, 2018.
- Abhishek Gupta, Vikash Kumar, Corey Lynch, Sergey Levine, and Karol Hausman. Relay policy learning: Solving long-horizon tasks via imitation and reinforcement learning. *arXiv preprint arXiv:1910.11956*, 2019.
- Tuomas Haarnoja, Aurick Zhou, Pieter Abbeel, and Sergey Levine. Soft actor-critic: Off-policy maximum entropy deep reinforcement learning with a stochastic actor. In *International conference on machine learning*, pages 1861–1870. Pmlr, 2018.
- Jonathan Ho, Ajay Jain, and Pieter Abbeel. Denoising diffusion probabilistic models. *Advances in neural information processing systems*, 33:6840–6851, 2020.
- Audrey Huang, Wenhao Zhan, Tengyang Xie, Jason D Lee, Wen Sun, Akshay Krishnamurthy, and Dylan J Foster. Correcting the mythos of kl-regularization: Direct alignment without overoptimization via chi-squared preference optimization. *arXiv preprint arXiv:2407.13399*, 2024.
- Physical Intelligence, Kevin Black, Noah Brown, James Darpinian, Karan Dhabalia, Danny Driess, Adnan Esmail, Michael Equi, Chelsea Finn, Niccolo Fusai, Manuel Y. Galliker, Dibya Ghosh, Lachy Groom, Karol Hausman, Brian Ichter, Szymon Jakubczak, Tim Jones, Liyiming Ke, Devin LeBlanc, Sergey Levine, Adrian Li-Bell, Mohith Mothukuri, Suraj Nair, Karl Pertsch, Allen Z. Ren, Lucy Xiaoyang Shi, Laura Smith, Jost Tobias Springenberg, Kyle Stachowicz, James Tanner, Quan Vuong, Homer Walke, Anna Walling, Haohuan Wang, Lili Yu, and Ury Zhilinsky. $\pi_{0.5}$: a vision-language-action model with open-world generalization, 2025. URL <https://arxiv.org/abs/2504.16054>.
- Diederik P Kingma and Max Welling. Auto-encoding variational bayes. *arXiv preprint arXiv:1312.6114*, 2013.
- Kun Lei, Huanyu Li, Dongjie Yu, Zhenyu Wei, Lingxiao Guo, Zhennan Jiang, Ziyu Wang, Shiyu Liang, and Huazhe Xu. Rl-100: Performant robotic manipulation with real-world reinforcement learning. *arXiv preprint arXiv:2510.14830*, 2025.
- Qiyang Li, Zhiyuan Zhou, and Sergey Levine. Reinforcement learning with action chunking. *arXiv preprint arXiv:2507.07969*, 2025.
- Yaron Lipman, Ricky TQ Chen, Heli Ben-Hamu, Maximilian Nickel, and Matt Le. Flow matching for generative modeling. *arXiv preprint arXiv:2210.02747*, 2022.
- Bo Liu, Yifeng Zhu, Chongkai Gao, Yihao Feng, Qiang Liu, Yuke Zhu, and Peter Stone. Libero: Benchmarking knowledge transfer for lifelong robot learning. *Advances in Neural Information Processing Systems*, 36:44776–44791, 2023.
- Jie Liu, Gongye Liu, Jiajun Liang, Yangguang Li, Jiaheng Liu, Xintao Wang, Pengfei Wan, Di Zhang, and Wanli Ouyang. Flow-grpo: Training flow matching models via online rl. *arXiv preprint arXiv:2505.05470*, 2025.
- Xingchao Liu, Chengyue Gong, and Qiang Liu. Flow straight and fast: Learning to generate and transfer data with rectified flow. *arXiv preprint arXiv:2209.03003*, 2022.
- Ajay Mandlekar, Danfei Xu, Josiah Wong, Soroush Nasiriany, Chen Wang, Rohun Kulkarni, Li Fei-Fei, Silvio Savarese, Yuke Zhu, and Roberto Martín-Martín. What matters in learning from offline human demonstrations for robot manipulation. In *arXiv preprint arXiv:2108.03298*, 2021.

- Max Sobol Mark, Tian Gao, Georgia Gabriela Sampaio, Mohan Kumar Srirama, Archit Sharma, Chelsea Finn, and Aviral Kumar. Policy agnostic rl: Offline rl and online rl fine-tuning of any class and backbone. *arXiv preprint arXiv:2412.06685*, 2024.
- David McAllister, Songwei Ge, Brent Yi, Chung Min Kim, Ethan Weber, Hongsuk Choi, Haiwen Feng, and Angjoo Kanazawa. Flow matching policy gradients. *arXiv preprint arXiv:2507.21053*, 2025.
- Leland McInnes, John Healy, and James Melville. Umap: Uniform manifold approximation and projection for dimension reduction. *arXiv preprint arXiv:1802.03426*, 2018.
- Mitsuhiko Nakamoto, Oier Mees, Aviral Kumar, and Sergey Levine. Steering your generalists: Improving robotic foundation models via value guidance. *Conference on Robot Learning (CoRL)*, 2024.
- Junhyuk Oh, Yijie Guo, Satinder Singh, and Honglak Lee. Self-imitation learning. In *International conference on machine learning*, pages 3878–3887. PMLR, 2018.
- Long Ouyang, Jeffrey Wu, Xu Jiang, Diogo Almeida, Carroll Wainwright, Pamela Mishkin, Chong Zhang, Sandhini Agarwal, Katarina Slama, Alex Ray, et al. Training language models to follow instructions with human feedback. *Advances in neural information processing systems*, 35:27730–27744, 2022.
- Chaoyi Pan, Giri Anantharaman, Nai-Chieh Huang, Claire Jin, Daniel Pfrommer, Chenyang Yuan, Frank Permenter, Guannan Qu, Nicholas Boffi, Guanya Shi, et al. Much ado about noising: Dispelling the myths of generative robotic control. *arXiv preprint arXiv:2512.01809*, 2025.
- Xue Bin Peng, Aviral Kumar, Grace Zhang, and Sergey Levine. Advantage-weighted regression: Simple and scalable off-policy reinforcement learning. *arXiv preprint arXiv:1910.00177*, 2019.
- Ethan Perez, Florian Strub, Harm De Vries, Vincent Dumoulin, and Aaron Courville. Film: Visual reasoning with a general conditioning layer. In *Proceedings of the AAAI conference on artificial intelligence*, volume 32, 2018.
- Karl Pertsch, Kyle Stachowicz, Brian Ichter, Danny Driess, Suraj Nair, Quan Vuong, Oier Mees, Chelsea Finn, and Sergey Levine. Fast: Efficient action tokenization for vision-language-action models. *arXiv preprint arXiv:2501.09747*, 2025.
- Yury Polyanskiy and Yihong Wu. *Information Theory: From Coding to Learning*. Cambridge University Press, 2025.
- Allen Z Ren, Justin Lidard, Lars L Ankile, Anthony Simeonov, Pulkit Agrawal, Anirudha Majumdar, Benjamin Burchfiel, Hongkai Dai, and Max Simchowitz. Diffusion policy policy optimization. *arXiv preprint arXiv:2409.00588*, 2024.
- Robin Rombach, Andreas Blattmann, Dominik Lorenz, Patrick Esser, and Björn Ommer. High-resolution image synthesis with latent diffusion models. In *Proceedings of the IEEE/CVF conference on computer vision and pattern recognition*, pages 10684–10695, 2022.
- John Schulman, Sergey Levine, Pieter Abbeel, Michael Jordan, and Philipp Moritz. Trust region policy optimization. In *International conference on machine learning*, pages 1889–1897. PMLR, 2015.
- John Schulman, Filip Wolski, Prafulla Dhariwal, Alec Radford, and Oleg Klimov. Proximal policy optimization algorithms. *arXiv preprint arXiv:1707.06347*, 2017.
- Amrith Setlur, Matthew YR Yang, Charlie Snell, Jeremy Greer, Ian Wu, Virginia Smith, Max Simchowitz, and Aviral Kumar. e3: Learning to explore enables extrapolation of test-time compute for llms. *arXiv preprint arXiv:2506.09026*, 2025.

- Zhihong Shao, Peiyi Wang, Qihao Zhu, Runxin Xu, Junxiao Song, Xiao Bi, Haowei Zhang, Mingchuan Zhang, YK Li, Yang Wu, et al. Deepseekmath: Pushing the limits of mathematical reasoning in open language models. *arXiv preprint arXiv:2402.03300*, 2024.
- Jiaming Song, Chenlin Meng, and Stefano Ermon. Denoising diffusion implicit models. *arXiv preprint arXiv:2010.02502*, 2020.
- Yang Song, Prafulla Dhariwal, Mark Chen, and Ilya Sutskever. Consistency models. 2023.
- Hyung Ju Suh, Max Simchowitz, Kaiqing Zhang, and Russ Tedrake. Do differentiable simulators give better policy gradients? In *International Conference on Machine Learning*, pages 20668–20696. PMLR, 2022.
- Ikechukwu Uchendu, Ted Xiao, Yao Lu, Banghua Zhu, Mengyuan Yan, Joséphine Simon, Matthew Ben- nice, Chuyuan Fu, Cong Ma, Jiantao Jiao, et al. Jump-start reinforcement learning. In *International Conference on Machine Learning*, pages 34556–34583. PMLR, 2023.
- Andrew Wagenmaker, Mitsuhiko Nakamoto, Yunchu Zhang, Seohong Park, Waleed Yagoub, Anusha Nagabandi, Abhishek Gupta, and Sergey Levine. Steering your diffusion policy with latent space reinforcement learning. *arXiv preprint arXiv:2506.15799*, 2025.
- Homer Walke, Kevin Black, Abraham Lee, Moo Jin Kim, Max Du, Chongyi Zheng, Tony Zhao, Philippe Hansen-Estruch, Quan Vuong, Andre He, Vivek Myers, Kuan Fang, Chelsea Finn, and Sergey Levine. Bridgedata v2: A dataset for robot learning at scale. In *Conference on Robot Learning (CoRL)*, 2023.
- Ronald J Williams. Simple statistical gradient-following algorithms for connectionist reinforcement learning. *Machine learning*, 8(3):229–256, 1992.
- Rosa Wolf, Yitian Shi, Sheng Liu, and Rania Rayyes. Diffusion models for robotic manipulation: A survey. *Frontiers in Robotics and AI*, 12:1606247, 2025.
- Yinfei Yang, Daniel Cer, Amin Ahmad, Mandy Guo, Jax Law, Noah Constant, Gustavo Hernandez Abrego, Steve Yuan, Chris Tar, Yun-Hsuan Sung, Brian Strope, and Ray Kurzweil. Multilingual universal sentence encoder for semantic retrieval, 2019. URL <https://arxiv.org/abs/1907.04307>.
- Brent Yi, Hongsuk Choi, Himanshu Gaurav Singh, Xiaoyu Huang, Takara E Truong, Carmelo Sferrazza, Yi Ma, Rocky Duan, Pieter Abbeel, Guanya Shi, et al. Flow policy gradients for robot control. *arXiv preprint arXiv:2602.02481*, 2026.
- Fan Zhang and Michael Gienger. Affordance-based robot manipulation with flow matching. *arXiv preprint arXiv:2409.01083*, 2024.
- Thomas T Zhang, Daniel Pfrommer, Nikolai Matni, and Max Simchowitz. Imitation learning in continuous action spaces: Mitigating compounding error without interaction. *arXiv preprint arXiv:2507.09061*, 2025a.
- Tonghe Zhang, Chao Yu, Sichang Su, and Yu Wang. Re inflow: Fine-tuning flow matching policy with online reinforcement learning. *arXiv preprint arXiv:2505.22094*, 2025b.
- Tony Z Zhao, Vikash Kumar, Sergey Levine, and Chelsea Finn. Learning fine-grained bimanual manipulation with low-cost hardware. *arXiv preprint arXiv:2304.13705*, 2023.
- Zhiyuan Zhou, Andy Peng, Qiyang Li, Sergey Levine, and Aviral Kumar. Efficient online reinforcement learning fine-tuning need not retain offline data. *arXiv preprint arXiv:2412.07762*, 2024.

Contents

1	Introduction	2
2	Preliminaries	3
3	Off-Policy Generative Policy Optimization	4
4	Improving OGPO by Mitigating Critic Over-exploitation	7
4.1	Vanilla OGPO Over-exploits Imperfectly Learned Critics	8
4.2	OGPO+ : Regularizing OGPO With Behavior Cloning of Successful Trajectories	9
4.3	OGPO+CA : Mitigating the Offline-to-Online Performance Dip via Conservative Advantages	10
4.4	OGPO+χ^2 : Overcoming critic exploitation on images via χ^2 regularization	11
5	When does Full-Finetuning (OGPO) Improve Over Popular Baselines?	11
5.1	Experimental Setup	12
5.2	Comparison to other methods	12
6	Understanding and Ablating The Merits of OGPO	14
6.1	Does OGPO Encourage Exploration?	14
6.2	Which Design Decisions Explain the Performance of OGPO and OGPO+ ?	15
6.3	Does PPO policy extraction outperform AWR and FPO extraction?	16
7	Related Work	16
7.1	Generative Control Policies	17
7.2	Reinforcement Learning for Robotic Policy Finetuning	17
7.3	Finetuning Strategies for Iterative Generative Policies	18
8	Conclusion and Limitations	18
A	A Practitioner’s Guide to OGPO	25
A.1	Key Design Decisions	25
B	Pseudocode	28
C	Generative Control Policies (GCPs): A Unifying Abstraction	30
C.1	OGPO with Diffusion Policies	31
C.2	Shortcut Policies	31
C.3	Minimal Iterative Policy	32
C.4	Tokenized Autoregressive Policies	32
D	Bi-Level MDP	33
E	Derivations	34
E.1	Policy Gradient Loss	34
E.2	Preventing Over-exploitation with χ^2 -Regularization	35
E.3	ODE-to-SDE Exploration Noise Correction	35
F	Baselines	36
F.1	Diffusion Policy Policy Optimization (DPPO , Ren et al. [2024])	37
F.2	Diffusion Steering Reinforcement Learning (DSRL , Wagenmaker et al. [2025])	37

F.3	Expressive Policy Optimization (EXPO , Dong et al. [2025])	38
F.4	Q-Chunking (QC , Li et al. [2025])	38
	F.4.1 Q-Chunking v/s OGPO	39
F.5	ReinFlow (Zhang et al. [2025b], not compared)	39
F.6	PA-RL (Mark et al. [2024], not compared)	39
G	Understanding Exploration Behavior of OGPO	39
H	Ablations and Limitations of OGPO/OGPO+	41
H.1	BPTT vs OGPO	41
H.2	OGPO v/s OGPO+ , with and without GRPO std (σ)	42
H.3	OGPO vs. OGPO with no-negative gradients	42
H.4	OGPO vs Steering + Residual Ablation	43
H.5	Policy Extraction Alternatives (AWR, ASPO from FPO)	43
	H.5.1 Advantage-Weighted Regression and Advantage-Weighted OGPO	43
	H.5.2 ASPO from Flow Policy Optimization	43
I	Environment Details	44
I.1	FRANKA-KITCHEN	44
I.2	Robomimic	45
I.3	Adroit Hand	46
I.4	LIBERO	46
J	Hyper-parameters and Initialization	47
J.1	Initialization and Warm Starting	47
J.2	Hyperparameters	48

A A Practitioner’s Guide to OGPO

In this section, we enumerate key design decisions, diagnostic tools, and configurations to serve as a reference for practitioners deploying **OGPO** on new tasks. We defer the pseudocode to [Appendix B](#) and the low level hyperparameters to [Appendix J](#)

A.1 Key Design Decisions

While a large set of hyperparameters remain static across all our experiments, some configurations might have a large impact on **OGPO**’s performance on tasks beyond the scope of this paper. We list each item by descending priority level denoted by its high level description followed by the variable name in the official code base.

0. Action Chunking Conventions and Critic Update The main paper denotes each action chunk $a_{t:t+h-1}$ simply as a_t for simplicity. Here we describe how this affects our computation of reward when used to train the resulting Q-function. Let us consider a standard MDP formulation where s_t is the state at current step, and $a_{t:t+h-1}$ denotes the action chunk. We follow the value backup formulation proposed in Q-chunking [Li et al., 2025], where the target uses an h -step return over the chunk and bootstraps from the value of the next action chunk at state s_{t+h} , with $a_{t+h:t+2h} \sim \pi_{\theta}(\cdot | s_{t+h})$ and $\bar{\theta}$ denoting the parameters of the target network. We use this loss to train the critic for all our off-policy methods, including **OGPO**, **QC**, **DSRL**, and **EXPO**:

$$L_{\text{critic}}(\theta) = \mathbb{E}_{s_t, a_{t:t+h}, s_{t+h} \sim \mathcal{B}} \left[\left(Q_{\theta}(s_t, a_{t:t+h}) - \underbrace{\sum_{t'=1}^h \gamma^{t'} r_{t+t'}}_{\text{effective reward}} - \gamma^h Q_{\text{targ}}(s_{t+h}, a_{t+h:t+2h}) \right)^2 \right]. \quad (\text{A.1})$$

Algorithmic Choices

1. Behavior-cloning regularization from the success buffer (bc_coeff). The total objective $L_{\text{Total}} = L_{\text{PPO}} + \lambda_{\text{BC}} L_{\text{BC}}$ (Eq. (4.3)) anchors the policy to actions from $\mathcal{D}_{\text{succ}} \subseteq \mathcal{D}_{\text{roll}}$ — the subset of replay-buffer transitions belonging to successful episodes. The regularizer is asymmetric: it raises the likelihood of empirically successful actions but never lowers the likelihood of failed ones, so L_{BC} contributes a strict lower bound on the modes L_{PPO} is allowed to abandon. Empirically (Figure 26) this is the single most consequential modification distinguishing **OGPO** from **OGPO+**. In all experiments, we typically select $\lambda = 1.0$.

2. Conservative advantages (adv_strategy=conservative, Eq. (4.5)). The conservative advantage \hat{A}_i^{cons} is non-zero if and only if all M ensemble members agree on the sign of $A_{i,m}$, in which case it takes the smallest magnitude consistent with that sign. Two consequences follow: (i) actions on which the ensemble disagrees produce no policy gradient, so the policy is updated only along directions of ensemble consensus; (ii) on directions of consensus, the magnitude is bounded by the most pessimistic Q-function, reducing the impact of outliers in the initial stages of online RL. This significantly mitigates the dip in policy evaluation and yields stable policy extraction.

3. Critic aggregation for Q_{targ} and Best-of- N (q_agg). As referenced in Algorithm 5, **OGPO** updates the critic ensemble by minimizing the Temporal Difference (TD) error. To calculate the target values,

we employ an ensemble of M target critic networks. The specific method for aggregating these target predictions is determined by the configuration flag `critic_flag`:

$$Q_{\text{targ}}(s', a') = \begin{cases} \min\{Q_{\phi_{i_1}}(s', a'), Q_{\phi_{i_2}}(s', a')\} & \text{critic_flag} = \mathbf{subsample} \\ \min_{i \in [M]} Q_{\phi_i}(s', a') & \text{critic_flag} = \mathbf{min} \\ \frac{1}{M} \sum_{i=1}^M Q_{\phi_i}(s', a') & \text{critic_flag} = \mathbf{mean} \end{cases} \quad (\text{A.2})$$

The setting of `critic_flag` is optimized per environment (see 5). The **min** flag uses the minimum all Q networks, which is more aggressively curtails overestimation. The **mean** flag uses the mean, which is less aggressive. Many works have found **subsample** to be a happy medium: we take the minimum of two critic networks whose indices i_1, i_2 are sampled uniformly from the ensemble $\{1, \dots, M\}$, individually per action. Note that critic training is agnostic to the GCP structure of the policy (Mark et al. [2024]).

Eq. (A.2) aggregates the critic ensemble $\{Q_{\bar{\phi}_m}\}_{m=1}^M$ via $f \in \{\text{mean}, \text{min}, \text{subsample}\}$. Across almost all tasks, we find `subsample` being the best strategy for Q_{targ} computation when using synchronous Jax updates, but `mean` to work best using asynchronous updates. Our experiments are run on using synchronous updates. In both cases, we also find `subsample` to work optimally for selected the Best-of- N actions Eq. (4.4).

4. ODE-to-SDE conversion (error_correct_sde_to_ode). In **OGPO**, we add Gaussian noise of variance σ^2 at each flow step to (1) ensure non-singular likelihoods thereby (2) facilitating exploration during online RL. Instead of the classic flow deterministic update $a_{t,k+1} = a_{t,k} + v_\theta(a_{t,k}, t_k)\Delta t$, where Δt is the discretization size. A naive approach would be to sample

$$a_{t,k+1} \sim \mathcal{N}(a_{t,k} + (v_\theta(a_{t,k}, t_k | s_t)\Delta t, \sigma^2 I), \quad (\text{A.3})$$

but this additional noise can cause distribution shift through the denoising chain, causing the policy with SDE inference to take different actions (and thus visit different states) than with ODE inference. Instead, we adopt a correction that mitigates distribution shift in the infinite-discretization step limit, also adopted by Liu et al. [2025]. Specifically, we learn a small score network

$$\hat{z}_\theta(\tilde{x}_t, t) \text{ by minimizing } L_{\text{denoiser}} = \mathbb{E}_{t, x_t, z} [\|\hat{z}_\theta(x_t + \sigma z, t) - z\|^2], \quad z \sim \mathcal{N}(0, \mathbf{I}), \quad (\text{A.4})$$

Then, we sample

$$a_{t,k+1} \sim \mathcal{N}\left(a_{t,k} + (v_\theta(a_{t,k}, t_k | s_t) + \frac{\sigma}{2\Delta t}(\hat{z}_\theta(a_{t,k}, t_k | s_t)\Delta t, \sigma^2 I)\right). \quad (\text{A.5})$$

In Appendix E.3, we show that this update produces samples with the same per-denoising-step marginal distribution as the original flow model, in the limit of infinite discretization and perfect learning of the score network, thereby validating this decision. Ablations in Figure 21 reveal the merits of this above sampling correction.

5. χ^2 -regularization to prevent Q-function overoptimization (Eq. (4.6)). Q-functions learned in the early stages of training tend to represent overly optimistic estimates at the fringes of the base policy coverage. χ^2 -regularization on the advantages (Appendix E.2) prevents overoptimization of Q functions, resulting in convergence for image-based **OGPO** runs. The GCP denoising chain already computes the per-step likelihoods needed to evaluate ω_θ , making this nearly free to implement during policy extraction. The penalty coefficient is set adaptively from the ensemble spread, $\beta = \beta_{\text{init}} \cdot \text{std}_m(Q_{\bar{\phi}_m}(s, a))$,

so that regularization is directly proportional to the critic disagreement. Further, we auto-calibrate Q_{targ} for the actor and the critic update as,

$$\begin{aligned}\psi(\omega_\theta) &= \sigma(\alpha(\omega_\theta - 1)), \\ Q_{\text{targ}} &= (1 - \psi(\omega_\theta)) \text{mean}_m(Q_{\bar{\phi}_m}) + \psi(\omega_\theta) \min_m(Q_{\bar{\phi}_m}),\end{aligned}\tag{A.6}$$

where $\psi(\omega_\theta)$ is a pessimism coefficient, σ is the Sigmoid operator, and α is a sensitivity parameter.

Hyperparameters

1. Group size N_{group} (`grpо_num_samples`). We rollout N_{group} trajectories in parallel from a single s_t to compute a mean value estimate for advantage computation in Eq. (3.2). Larger N_{group} values result in higher exploration and diversity of information points at each update at the cost of compute. We find $N_{\text{group}} = 32$ to be a sweet spot across all our experiments.

2. PPO clip ϵ (`clip_epsilon`). The Annealed Importance Sampling ratio ω computed in Eq. (3.2) is sensitive to small perturbations in the likelihoods of each denoising step of the GCP being used. For 10-step flow policies, we find a clipping value of $\epsilon = 0.01$ to work best for stable policy extraction. However, practitioners might need to experiment with this ratio depending on their GCP policy parameterization.

3. Update-to-data ratios We provide three key update-to-data (UTD) ratios – `utd_warmup` (number of critic updates per base policy rollout step), `utd_q` (number of critic updates per online policy rollout step), and `utd_pi` (number of actor updates per online policy rollout step). Although a UTD of 1 works across the board, they can be tweaked individually depending on the task setting.

4. Exponential Moving Average For all GCP instantiations within **OGPO**, we maintain an Exponential Moving Average (EMA) of the policy weights, denoted as θ_{EMA} . At every training step, after updating θ , we update θ_{EMA} via:

$$\theta_{\text{EMA}} \leftarrow \alpha \theta_{\text{EMA}} + (1 - \alpha) \theta,\tag{A.7}$$

where α is a decay rate we typically set $\alpha = 0.995$. For **OGPO**, the EMA serves a dual purpose beyond standard stability. First, it acts as the reference policy $\pi_{\theta_{\text{old}}}$ in the PPO importance sampling ratio (Eq. (3.2)), ensuring that updates are constrained relative to a stable baseline rather than the rapidly changing online policy. Second, for the planning component in **OGPO+**, trajectories for Best-of-N ranking are sampled using $\pi_{\theta_{\text{EMA}}}$ to ensure stability in the candidate actions.

B Pseudocode

Algorithm 2 OGPO+

```

1:  $\bar{\pi}_\theta, Q_{\phi_{1..M}}, \mathcal{D}_{\text{roll}} \leftarrow \emptyset, \mathcal{D}_{\text{succ}} \leftarrow \emptyset$ 
2:  $\theta_{\text{targ}} \leftarrow \theta, \phi_{\text{targ},i} \leftarrow \phi_i \quad \forall i \in \{1, 2, \dots, M\}$ 
3: for iteration = 1, 2, ... do
4:   Initialize state  $s_{t=0} = s_0$  in  $M_{\text{ENV}}$ 
5:    $\mathcal{T}_{\text{ep}} \leftarrow \emptyset$  Temporary episode buffer
6:   while not done do
7:      $(s, a, r, s', \text{done}) \leftarrow \text{TAKE\_STEP}$  from the environment
8:      $\mathcal{D}_{\text{roll}} \leftarrow \mathcal{D}_{\text{roll}} \cup \{(s, a, r, s', \text{done})\}$ 
9:      $\mathcal{T}_{\text{ep}} \leftarrow \mathcal{T}_{\text{ep}} \cup \{(s, a, r, s', \text{done})\}$ 
10:    % Update critic and policy
11:    for epoch = 1, 2, ..., utd do
12:      if use_offline then
13:         $B_{\text{itr}} \sim \{r_{\text{offline}} \mathcal{D}_{\text{off}} \cup (1 - r_{\text{offline}}) \mathcal{D}_{\text{roll}}\}$ 
14:      else
15:         $B_{\text{itr}} \sim \mathcal{D}_{\text{roll}}$ 
16:      end if
17:       $B_{\text{succ}} \sim \mathcal{D}_{\text{succ}}$  if  $\mathcal{D}_{\text{succ}} \neq \emptyset$ 
18:      UPDATEQ( $B_{\text{itr}}$ )
19:      UPDATEIGP( $B_{\text{itr}}, B_{\text{succ}}$ )
20:      %Update target networks:
21:       $\phi_{\text{targ},i} \leftarrow (1 - \tau)\phi_i + \tau\phi_{\text{targ},i} \quad \forall i \in 1, \dots, M$ 
22:       $\theta_{\text{targ}} \leftarrow (1 - \tau)\theta + \tau\theta_{\text{targ}}$ 
23:    end for
24:  end while
25:  if episode successful then
26:     $\mathcal{D}_{\text{succ}} \leftarrow \mathcal{D}_{\text{succ}} \cup \mathcal{T}_{\text{ep}}$   $\mathcal{D}_{\text{succ}} \subseteq \mathcal{D}_{\text{roll}}$ 
27:  end if
28: end for
29: return converged policy  $\pi_\theta$ 

```

Algorithm 3 Initialization

```

1: Function INITIALIZE( $\mathcal{D}_{\text{off}}$ )
2: {% Policy Initialization}
3: Pre-train IGP  $\bar{\pi}_{\theta}^{\text{BC}}$  on  $\mathcal{D}_{\text{off}}$  using BC loss  $\mathcal{L}_{\text{BC}}(\theta)$ 
4:  $\bar{\pi}_{\theta} \leftarrow \bar{\pi}_{\theta}^{\text{BC}}$ 
5: {% Critic Initialization}
6: Initialize ensemble of Q functions  $Q_{\phi_{1..M}}$ 
7: if use_calql then
8:   Pre-train  $Q_{\phi_{1..M}}$  on  $\mathcal{D}_{\text{off}}$  using  $\mathcal{L}_{\text{critic}}$  {Optional offline RL}
9: end if
10: {% Buffer Initialization}
11:  $\mathcal{D}_{\text{roll}} \leftarrow \emptyset$ 
12:  $\mathcal{D}_{\text{succ}} \leftarrow \emptyset$ 
13: {% Warmup Rollouts}
14: for episode = 1, ...,  $N_{\text{warmup}}$  do
15:   Roll out  $\bar{\pi}_{\theta}^{\text{BC}}$  in  $M_{\text{ENV}}$ , collect transitions
16:    $\mathcal{D}_{\text{roll}} \leftarrow \mathcal{D}_{\text{roll}} \cup \{(s, a, r, s', \text{done})\}_{\text{episode}}$ 
17:   if episode successful then
18:      $\mathcal{D}_{\text{succ}} \leftarrow \mathcal{D}_{\text{succ}} \cup \{(s, a, r, s', \text{done})\}_{\text{episode}}$ 
19:   end if
20: end for
21: if warmup_critic then
22:   for step = 1, ...,  $N_{\text{critic\_warmup}}$  do
23:      $B_{\text{itr}} \sim \mathcal{D}_{\text{roll}}$ 
24:     UPDATEQ( $B_{\text{itr}}$ ) {Critic-only updates}
25:   end for
26: end if
27:
28: return  $\bar{\pi}_{\theta}, Q_{\phi_{1..M}}, \mathcal{D}_{\text{roll}}, \mathcal{D}_{\text{succ}}$ 

```

Algorithm 4 Take A Step In The Environment

```

1: Function TAKE_STEP( $s_t$ )
2: done  $\leftarrow$  False
3:  $a_{t,K} \sim \text{N}(0,1)$ 
4: for  $k = K, \dots, 0$  do
5:    $a_{t,k-1} \leftarrow \bar{\pi}_{\theta_{\text{targ}}}(a_k, k, s_t)$ 
6: end for
7:  $r, s_{t+1} \leftarrow$  Execute  $a_{t,0}$  in environment
8: if  $s_{t+1}$  is terminal then
9:   done  $\leftarrow$  True
10: end if
11:
12: return ( $s_t, a_{t,0}, r, s_{t+1}, \text{done}$ )

```

Algorithm 5 Critic Update

- 1: **Function** UPDATEQ(B_{itr})
 - 2: $(s_t, a_{t,0}, r, s_{t+1}, \text{done}) \leftarrow B_{\text{itr}}$
 With θ frozen:
 - 3: $a_{t+1,0} \leftarrow \pi_{\theta_{\text{targ}}}(\cdot | s_{t+1})$
 - 4: $y \leftarrow r + \gamma \cdot \mathbb{I}[\text{not done}] \cdot Q_{\text{targ}}(s_{t+1}, a_{t+1,0})$ {Ref. Eq. A.2}
 - Update $\phi_{1,\dots,M}$ via gradient descent:
 - 5: $\nabla_{\phi_i} \frac{1}{|B_{\text{itr}}|} \sum_{B_{\text{itr}}} (Q_{\phi_i}(s_t, a_{t,0}) - y)^2$ for $i = 1, \dots, M$
-

Algorithm 6 IGP Update

- 1: **Function** UPDATEIGP($B_{\text{itr}}, B_{\text{succ}}$)
 On-Policy PPO Update
 - 2: $s_t \leftarrow B_{\text{itr}}$
 - 3: Sample G actions: $\{\bar{\tau}^{(g)}\}_{g=1}^G \sim \pi_{\theta_{\text{targ}}}(\cdot | s_t)$
 - 4: $\hat{A}^G = Q_{\text{targ}}(s_t, a_{t,0}^G) - \mu(Q_{\text{targ}}(s_t, a_{t,0}^G))$
 - 5: $\omega_\theta = \frac{\prod_{k=K}^0 \bar{\pi}_\theta^G(a_{t,k-1} | a_k, k, s_t)}{\prod_{k=K}^0 \bar{\pi}_{\theta_{\text{targ}}}^G(a_{t,k-1} | a_k, k, s_t)}$
 - 6: $\mathcal{L}_{\text{PPO}}(\theta) = \mathbb{E}_{\bar{\tau} \sim \pi_{\theta_{\text{targ}}}} \left[\min(\omega_\theta \cdot \hat{A}^G, \text{clip}(\omega_\theta, 1 - \epsilon, 1 + \epsilon) \cdot \hat{A}^G) \right]$
 BC Update from Success Buffer
 - 7: $(s_t^{\text{succ}}, a_{t,0}^{\text{succ}}) \leftarrow B_{\text{succ}}$
 - 8: $\mathcal{L}_{\text{BC}}(\theta) = \text{BCLoss}(\bar{\pi}_\theta(\cdot | s_t^{\text{succ}}), a_{t,0}^{\text{succ}})$ {IGP-specific}
 - Combined Update
 - 9: $\mathcal{L}_{\text{total}}(\theta) = \mathcal{L}_{\text{PPO}}(\theta) + \lambda_{\text{BC}} \mathcal{L}_{\text{BC}}(\theta)$
 - 10: Update θ via gradient descent on $\mathcal{L}_{\text{total}}(\theta)$
-

C Generative Control Policies (GCPs): A Unifying Abstraction

We propose a unifying abstraction for a broad family of popular parameterizations of control policies that we call *Iterative Generative Policies*, or **GCPs**. GCPs represent a stochastic policy $\pi_\theta(\cdot | s)$ as a series of iterative computation steps, defined by a mapping $\bar{\pi}_\theta : S \times A \times \mathbb{N}$. Given a state s_t , the policy samples $a_{t,K} \sim \bar{\pi}_\theta(\cdot | a_{t,k} = \emptyset, k = K, s_t)$. From then, we sample $a_{t,k-1} \sim \bar{\pi}_\theta(\cdot | a_{t,k}, k, s_t)$. The final action proposed is an action $a_{t,0}$. We compactly denote the distribution of this action given the observation as $a_{t,0} \sim \pi_\theta(\cdot | s_t)$, turning the GCP into a standard policy. Our iteration conventions are *decreasing* in K , following typical convention for diffusion models. We also drop t subscripts when clear from context.

Examples of GCPs: In addition to iterative computation, the only other requirement is that the conditional likelihoods, $\log \bar{\pi}_\theta(a_{t,k-1} = a | s_t, a_{t,k}, k)$ are efficiently represented. A number of popular parameterizations produce actions iteratively and satisfy this mild requirement:

- **Diffusion Policies** [Chi et al., 2023] use Denoising Diffusion Probabilistic Models (DDPMs) Ho et al. [2020]. Instantiated as an GCP, these take in pairs (s, a) as training data and iteratively add Gaussian noise to the actions through a forward process $q(a_{k+1} | a_k)$ and learn a function $\epsilon_\theta(a_k, k, s)$ predicting the noise added to convert x_0 to x_k . To produce an action, we sample $a_{t,K} \sim \text{N}(0, \mathbf{I})$, and iteratively generate denoised samples with the following reverse process:

$$a_{k-1} \sim \bar{\pi}^{\text{DDPM}}(\cdot | a_k, k, s) := \text{N}(\mu_k(x_k, \epsilon_\theta(a_k, k, s)), \sigma_k^2 \mathbf{I}) \quad (\text{C.1})$$

- **Flow policies** are based on flow matching models. Given training pairs (s, a) , we sample noise $z \sim N(0, \mathbf{I})$, and define the interpolant $a_{(\tau)} := \tau a + (1 - \tau)z$ with continuous noise index $\tau \in [0, 1]$. We then learn a velocity field $v_\theta(a_{(\tau)}, \tau, s)$, these predict $\mathbb{E}[a - z \mid s, a_{(\tau)}]$. For K discretization steps, we generate samples by initializing $a_0 \sim N(0, \mathbf{I})$ and discretizing an ordinary differential equation (ODE) which reverses the noising process $a_{k-1} := a_k + \frac{1}{K}v_\theta(a_k, k/K, s)$. In its stand form, $a_{k-1} \mid a_k, s$ is deterministic. Thus, to convert a flow policy into a proper GCP, for which *likelihoods* are well-defined, we must add additional noise at each step (Reinflow [Zhang et al., 2025b]). For a given choice of noise levels σ_k^2 , this induces the GCP:

$$a_{k-1} \sim \bar{\pi}^{\text{FLOW}}(\cdot \mid a_k, k, s) := N(v_\theta(a_k, k/K, s), \sigma_k^2 \mathbf{I}) \quad (\text{C.2})$$

- **Minimal Iterative Policies (MIP)** are two-step flow policies which yield a performance comparable to 10-step flow policies with the natural benefit of allowing much faster inference. We defer the formal definition to Appendix C.3

The GCP formalism encompasses a number of more recent policy parameterizations as well, such as

- **Shortcut Policies** [Frans et al., 2024]: Flow models with learnable step sizes that enable variable-length generation trajectories.
- **Tokenized Autoregressive Policies (FAST)** [Pertsch et al., 2025]: Policies that tokenize continuous actions in Fourier space and generate them autoregressively as discrete sequences.

In the interest of brevity, we detail the above in the Appendix C.2, and Appendix C.4 respectively. Conveniently, the GCP formalism abstracts away the details of these varying instantiations, allowing us to state all algorithms cleanly.

C.1 OGPO with Diffusion Policies

OGPO can, in principle, be combined with any GCPs. Here, as an example, we illustrate its use in diffusion policies. We study this on the SQUARE task, where we pre-train a diffusion policy on the MH dataset and then apply online improvement with **OGPO**. As shown in Figure 19, **OGPO** successfully improves the diffusion policy to achieve mastery.

C.2 Shortcut Policies

Shortcut policies [Frans et al., 2024] are derived from flow-matching models conditioned on a step-size parameter d . The model $\bar{\pi}_\theta(a_t, t, d, o)$ learns to predict the next state of the flow a_{t+d} by taking a shortcut of size d . This allows the policy to function as an GCP with a variable number of refinement steps K . During pretraining, shortcut models utilize a self-consistency loss that enforces the property that one shortcut step of size $2d$ should be equivalent to two consecutive steps of size d :

$$\pi_\theta(a_t, t, 2d, o) \approx \frac{1}{2}\pi_\theta(a_t, t, d, o) + \frac{1}{2}\pi_\theta(a'_{t+d}, t + d, d, o) \quad (\text{C.3})$$

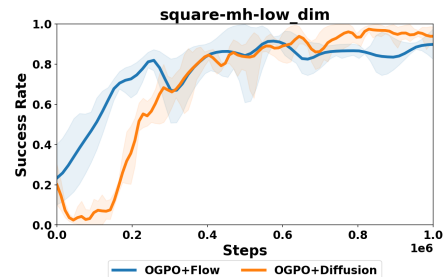


Figure 19: OGPO with diffusion policies. **OGPO** can successfully improve both flow policy and diffusion policy. We predominantly use flow policies due to the faster inference compute

C.3 Minimal Iterative Policy

Minimal Iterative Policies (MIP) [Pan et al., 2025] represent the simplest GCP instantiation that retains the performance benefits of flow-based policies. The key insight is that the success of generative control policies stems from combining *Stochasticity Injection* during training with *Supervised Iterative Computation*, rather than learning the distributions themselves. MIP uses only $K = 2$ denoising steps, with the first step computing $a_{t,1} \leftarrow \pi_\theta(s_t, a_{t,2} = \bar{0}, t = 0)$, then refining via $a_{t,0} \leftarrow \pi_\theta(s_t, t^* a_{t,1}, t^*)$. The core insight being that merely learning the conditional mean is sufficient to match the performance of complex flow-matching policies, provided the refinement steps allow the policy to adhere to the expert action manifold.

Formally, MIP optimizes the following objective during pretraining, where $t^* = 0.9$ and $z \sim \mathcal{N}(0, I)$ is injected noise:

$$\mathcal{L}_{\text{MIP}}(\theta) = \mathbb{E}[\|\pi_\theta(o, I_0 = 0, t = 0) - a\|^2 + \|\pi_\theta(o, I_{t^*}, t^*) - a\|^2], \quad (\text{C.4})$$

where I_{t^*} is the interpolant between action a and noise z .

C.4 Tokenized Autoregressive Policies

Tokenized policies, such as those using the FAST tokenizer [Pertsch et al., 2025], represent the action distribution via categorical distributions over a vocabulary of discrete tokens. FAST efficiently handles high-frequency continuous control data by applying a Discrete Cosine Transform (DCT) to action chunks, followed by quantization and Byte-Pair Encoding (BPE).

In this formulation, the GCP is an autoregressive Transformer $\bar{\pi}_\theta(z_k | z_{<k}, s_t)$, where z represents the sequence of discrete tokens corresponding to a compressed action chunk. The generative process iteratively samples tokens:

$$z_k \sim \text{Categorical}(\pi_\theta(\cdot | z_{<k}, o)) \quad (\text{C.5})$$

Unlike diffusion or flow policies where iteration occurs in continuous action space (refining the values), here iteration occurs in the token sequence space. In particular, this slightly deviates from the GCP formulation described in the main text by requiring conditioning on the whole token sequence $z_{<k}$. However, the light likelihoods in our PPO update in Eq. (3.3) can be easily modified to handle this setting, because $p(z_{1:k}) = \prod_k p(z_k | z_{<k})$.

D Bi-Level MDP

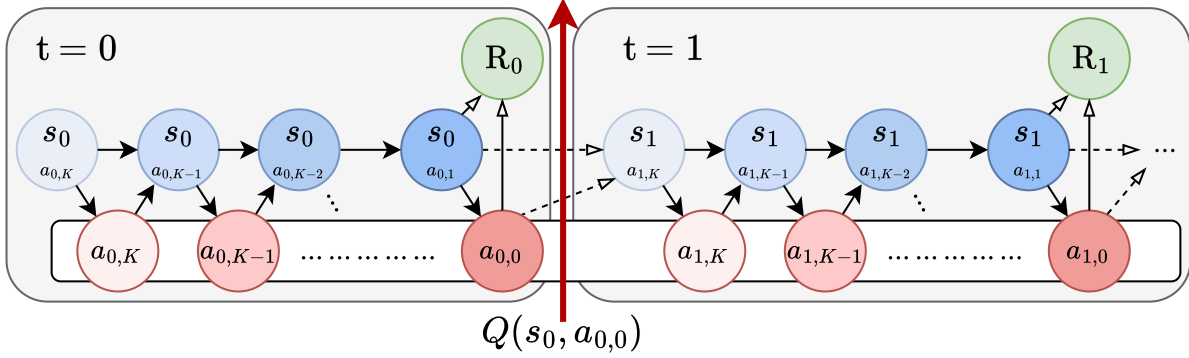


Figure 20: Bi-level (two-layer) MDP construction. Each environment step t is expanded into K inner action-generation steps indexed by $k \in \{K-1, \dots, 0\}$. The environment transitions and rewards occur only at $k=0$, while for $k > 0$ the state is unchanged and the inner action variable is updated.

We formulate the bi-level MDP (Figure 20), also called the two-layer MDP in [Ren et al., 2024], by embedding the action-generation dynamics into the environment dynamics. This yields an augmented MDP M_{BILEVEL} whose trajectory explicitly interleaves environment time with the K action-generation steps.

Recall the environment MDP $M_{\text{ENV}} := (S, A, P_0, P, R, \gamma)$ defined in Section 2. In M_{BILEVEL} , we index time by pairs (t, k) , where t denotes the environment step and $k \in \{0, \dots, K-1\}$ denotes the action-generation step, with $k=0$ corresponding to executing the final action in the environment. We map (t, k) to a single time index via $\bar{t}(t, k) = tK + (K - k - 1)$, so that the sequence $\bar{t}(t, K-1), \bar{t}(t, K-2), \dots, \bar{t}(t, 0)$ corresponds to the K generation/execution steps within environment step t . The state, action, and reward in M_{BILEVEL} are defined as

$$\bar{s}_{\bar{t}(t,k)} = (s_t, a_{t,k+1}), \quad \bar{a}_{\bar{t}(t,k)} = a_{t,k}, \quad \bar{R}_{\bar{t}(t,k)}(\bar{s}_{\bar{t}(t,k)}, \bar{a}_{\bar{t}(t,k)}) = \begin{cases} 0, & k > 0, \\ R(s_t, a_{t,0}), & k = 0. \end{cases}$$

Importantly, rewards are emitted only at indices corresponding to executing the environment action, i.e., when $a_{t,0}$ is taken. The initial distribution factorizes as $\bar{P}_0 = P_0 \otimes P_{\text{ACTION},0}$, where $s_0 \sim P_0$ is the initial environment state and $a_{0,K}$ is sampled independently from $P_{\text{ACTION},0}$, the initialization distribution for the action-generation process at $t=0$.

Finally, the transition kernel is given by

$$\bar{P}(\bar{s}_{\bar{t}+1} | \bar{s}_{\bar{t}}, \bar{a}_{\bar{t}}) = \begin{cases} \delta_{(s_t, a_{t,k})}, & \bar{t} = \bar{t}(t, k), k > 0 \\ P(\cdot | s_t, a_{t,0}) \otimes P_{\text{ACTION},t+1} & \bar{t} = \bar{t}(t, k), k = 0 \end{cases}$$

where $P_{\text{ACTION},t}$ (for $t \geq 0$) denotes the initialization distribution for $a_{t,K}$. Intuitively, when $k > 0$, the transition advances the iterative action-generation process by moving from $(s_t, a_{t,k+1})$ to $(s_t, a_{t,k})$ while keeping the environment state fixed; when $k=0$, it executes $a_{t,0}$ in the environment, samples $s_{t+1} \sim P(\cdot | s_t, a_{t,0})$, and re-initializes the next inner process by sampling $a_{t+1,K} \sim P_{\text{ACTION},t+1}$.

E Derivations

E.1 Policy Gradient Loss

An optimal policy parameterized by θ can be obtained by maximizing an objective function that computes the expected reward over a trajectory $\tau \sim \pi_\theta(\tau)$. Mathematically, $\theta^* = \arg \max_\theta J(\theta)$, where $J(\theta) = \mathbb{E}_{\tau \sim \pi_\theta(\tau)} [\omega(\tau)]$. Hence, the policy gradient objective is given as:

$$\nabla_\theta J(\theta) = \mathbb{E}_{\tau \sim \pi_\theta(\tau)} [\nabla_\theta \log \pi_\theta(\tau) \omega(\tau)] \quad (\text{E.1})$$

However, there are two main challenges which make the classical PG loss formulation challenging to converge in practice. (1) Policies parameterized as neural networks can only change a little with each gradient step. (2) High variance environments require a very large number of rollouts to obtain π^* , which is prohibitively expensive and potentially unsafe to do on real robots. As proposed by [Schulman et al., 2015], high variance can be mitigated by estimating an expectation under a distribution from an older policy $\pi_{\theta_{\text{old}}}$ using importance sampling (IS). This implies use of short horizon replay buffers where actions sampled under $\pi_{\theta_{\text{old}}}$ are reused to compute IS against π_θ . This modifies the PG objective as follows:

$$\begin{aligned} \nabla_\theta J(\theta) &= \mathbb{E}_{\tau \sim \pi_\theta(\tau)} \left[\frac{\pi_\theta(\tau)}{\pi_{\theta_{\text{old}}}(\tau)} \nabla_\theta \log \pi_\theta(\tau) \omega(\tau) \right] \\ &= \mathbb{E}_{\tau \sim \pi_\theta(\tau)} \left[\left(\sum_{t=1}^T \nabla_\theta \log \pi_\theta(a_t | s_t) \right) \left(\prod_{t=1}^T \frac{\pi_\theta(a_t | s_t)}{\pi_{\theta_{\text{old}}}(a_t | s_t)} \right) \left(\sum_{t=1}^T r(s_t, a_t) \right) \right] \end{aligned} \quad (\text{E.2})$$

However, the product of importance weights in the trajectory-level estimator leads to vanishing probability products for long horizons T . The objective is reformulated using state-action marginals. This separates the expectation over states (dependent on transition dynamics) from the expectation over actions (dependent on the policy):

$$J(\theta) = \sum_{t=1}^T \mathbb{E}_{s_t \sim \rho_{\theta_{\text{old}}}(s_t)} \left[\frac{\rho_\theta(s_t)}{\rho_{\theta_{\text{old}}}(s_t)} \mathbb{E}_{a_t \sim \pi_{\theta_{\text{old}}}(a_t | s_t)} \left[\frac{\pi_\theta(a_t | s_t)}{\pi_{\theta_{\text{old}}}(a_t | s_t)} r(s_t, a_t) \right] \right] \quad (\text{E.3})$$

Calculating the state density ratio $\frac{\rho_\theta(s_t)}{\rho_{\theta_{\text{old}}}(s_t)}$ is difficult as it requires knowledge of the system dynamics. Therefore, TRPO and PPO introduce a simplification by ignoring this term. This results in a biased estimator, but the bias is negligible provided π_θ remains close to $\pi_{\theta_{\text{old}}}$. The resulting surrogate objective maximizes the probability of actions with high rewards (or advantages) relative to the old policy:

$$J(\theta) \approx \sum_{t=1}^T \mathbb{E}_{s_t \sim \rho_{\theta_{\text{old}}}} \left[\mathbb{E}_{a_t \sim \pi_{\theta_{\text{old}}}} \left[\frac{\pi_\theta(a_t | s_t)}{\pi_{\theta_{\text{old}}}(a_t | s_t)} r(s_t, a_t) \right] \right] \quad (\text{E.4})$$

Classically, algorithms like PPO parameterize the policy $\pi_\theta(a|s)$ as a unimodal Gaussian distribution $\mathcal{N}(\mu_\theta(s), \Sigma)$. This yields a unimodal importance sampling ratio at every timestep t , which naturally struggles to model the multimodal action distributions necessary during RL exploration for complex manipulation tasks. Conversely, the total probability $\tilde{\pi}_\theta(a_{t,0} | s_t)$ in a GCP is the product of the transition probabilities along the generation steps k . This likelihood is given as: $\pi_\theta(a_{t,0} | s_t) = \prod_{k=1}^K \pi_\theta(a_{t,k} | s_t)$

Substituting this into the standard PPO objective requires computing the ratio of these products. While trajectory-level importance sampling is unstable for long environment MDP chains (where $T \approx 400 - 1000$), the denoising MDP horizon of the generative process can be sufficiently short (typically $K \leq 10$)

Assuming the current policy π_θ and the reference policy (typically an Exponential Moving Average, π_{EMA}) are close, we extend the TRPO formulation to the GCP chains to compute the Annealed Importance Sampling (AIS) ratio:

$$\omega_\theta := \prod_{k=1}^K \frac{\pi_\theta(a^{k-1} | s, a^k)}{\pi_{\theta_{\text{EMA}}}(a^{k-1} | s, a^k)} \quad (\text{E.5})$$

The probability of the final executed action is the joint probability of the entire chain: $\pi_\theta(a_{t,0} | s_t) = \prod_{k=K}^1 \pi(a_{t,k-1} | a_{t,k}, s_t)$. We substitute the Monte Carlo return $\omega(\tau)$ with the advantage \hat{A} , which yields the final **OGPO** objective described in Eq. (3.2). When multiplied with the advantage \hat{A} , the resulting gradients propagate to every step k , updating each in proportion to its contribution to the final action’s probability. This end-to-end formulation ensures that generating a high-value action $a_{t,0}$ requires coherent refinement at every step $a_{t,k}$ if the GCP.

E.2 Preventing Over-exploitation with χ^2 -Regularization

The following lemma shows that the modification of the advantage by the likelihood term, described in Eq. (4.6), is equivalent to χ^2 regularization:

Lemma E.1. *Let $P_\theta(s)$ denote the distribution over the denoising trajectory $a^K, \dots, a^0 \sim \pi_\theta(s)$, and $P_{\text{slow}}(s)$ denote the distribution over the denoising trajectory drawn from π_{slow} . Then,*

$$\mathbb{E}_{a^K, \dots, a^0 \sim \pi_\theta(s)}[\omega_\theta] = 1 + \chi^2(P_\theta(s), P_{\text{slow}}(s)). \quad (\text{E.6})$$

In particular, both sides of the above equation have the same gradients:

$$\nabla_\theta \mathbb{E}_{a^K, \dots, a^0 \sim \pi_\theta(s)}[\omega_\theta] = \nabla_\theta \chi^2(P_\theta(s), P_{\text{slow}}(s)) \quad (\text{E.7})$$

Proof. This follows from the definition of the χ^2 divergence [Polyanskiy and Wu, 2025]: if P, Q are two measures on a space X with densities p, q , then $1 + \chi^2(P, Q) = \int p(x)^2/q(x) dx = \mathbb{E}_{x \sim p}[p(x)/q(x)]$. Now take $x = (a^K, \dots, a^0)$ to be denoising trajectories, $p(x)$ the density under π_θ , and $q(x)$ the density under π_{slow} . \square

E.3 ODE-to-SDE Exploration Noise Correction

In order to have nondegenerate likelihoods, we need to convert deterministic flow inference into a stochastic process. Naively, we could add Gaussian noise (as in Zhang et al. [2025b]), but the addition of new noise introduces distribution shift between the original action distribution and the noise-augmented action distribution. We note that the same approach is also adopted by Liu et al. [2025].

Specifically, we follow Albergo et al. [2023], which provides a principled conversion from ODE inference (as in standard flow models) in an SDE). Consider a continuous-time ODE

$$\frac{d}{d\tau} X_\tau = v(X_\tau, \tau), \quad (\text{E.8})$$

where $v_\tau(x)$ is the flow velocity field. Next for a time varying diffusion coefficient ϵ_τ , define an stochastic differential equation (SDE)

$$dX_\tau^{\text{SDE}} = \underbrace{\left[v(X_\tau^{\text{SDE}}, \tau) + \epsilon(\tau) s(X_\tau^{\text{SDE}}, \tau) \right]}_{v^{\text{SDE}}(X_\tau^{\text{SDE}}, \tau)} d\tau + \sqrt{2\epsilon(\tau)} dW_t, \quad (\text{E.9})$$

where $s_\tau(x) = \nabla_x \log \rho_\tau(x)$ is the score function, and where ρ_τ is the marginal distribution of X_τ .

Proposition E.2 (Albergo et al. [2023]). *For every time τ , the marginal distribution of X_τ and X_τ^{SDE} are the same.*

The key insight is that the correction in the SDE drift $v_\tau^{\text{SDE}} = v_\tau + \epsilon_\tau s_\tau$ directly offsets the effect of the Brownian drift. Furthermore, by Tweedie’s formulation, the score function can be computed as

$$s(\tilde{x}_\tau, \tau) = \frac{1}{\sigma} (\mathbb{E}[Z \mid X_\tau + \sigma Z = \tilde{x}_\tau]), \quad Z \sim \mathcal{N}(0, \mathbf{I}) \quad (\text{E.10})$$

In particular, $s_\tau = \frac{1}{\sigma} z_\tau$, where

$$z_\tau \in \underset{z(\cdot)}{\text{arg min}} \mathbb{E} \|z_\tau(X_\tau + \sigma Z) - Z\|^2. \quad (\text{E.11})$$

Specialization to OGPO via discretization In OGPO, we add noise to each discrete step k with timestep Δt . Instead of the classic flow deterministic update $a_{t,k+1} = a_{t,k} + v_\theta(a_{t,k}, t_k) \Delta t$. A naive approach would be to sample:

$$a_{t,k+1} \sim \mathcal{N}(a_{t,k} + (v_\theta(a_{t,k}, t_k \mid s_t) \Delta t, \sigma^2 I)), \quad (\text{E.12})$$

which as, noted above, would cause distribution shift. Instead, we learn a small score network

$$\hat{z}_\theta(\tilde{x}_t, t) \text{ by minimizing } L_{\text{denoiser}} = \mathbb{E}_{t, x_t, z} [\|\hat{z}_\theta(x_t + \sigma z, t) - z\|^2], \quad z \sim \mathcal{N}(0, \mathbf{I}), \quad (\text{E.13})$$

and instead sample.

$$a_{t,k+1} \sim \mathcal{N}\left(a_{t,k} + (v_\theta(a_{t,k}, t_k \mid s_t) + \frac{\sigma}{2\Delta t} (\hat{z}_\theta(a_{t,k}, t_k \mid s_t) \Delta t, \sigma^2 I)), \quad (\text{E.14})$$

where σ is the standard deviation and v_θ is the learned velocity field. This update corresponds to the Euler-Maruyama discretization of the SDE

$$\frac{d}{d\tau} a_{t,\tau} = (v_\theta(a_{t,\tau}, \tau \mid s_t) + \frac{\epsilon}{\sigma} (z_\theta(a_{t,\tau}, t_\tau \mid s_t) + \sqrt{2\epsilon} dW_t), \quad (\text{E.15})$$

with diffusion coefficient set to $\epsilon = \sigma^2 / (2\Delta t)$. In the limit where \hat{z}_θ is the global minimizer of Eq. (E.13) under x_t drawn from the true flow ODE

$$\frac{d}{d\tau} a_{t,\tau} = v(a_{t,\tau}, \tau \mid s_t) \quad (\text{E.16})$$

The marginals of Eq. (E.15) and Eq. (E.16) coincide due to Proposition E.2 and the above discussion. Ablations in Figure 21 reveal the merits of this above sampling correction.

F Baselines

In this section, we describe all baselines we compare to in detail. Throughout, we adopt of the action-chunking conventions of Appendix A.1 . For the off-policy methods below (EXPO, QC, DSRL),

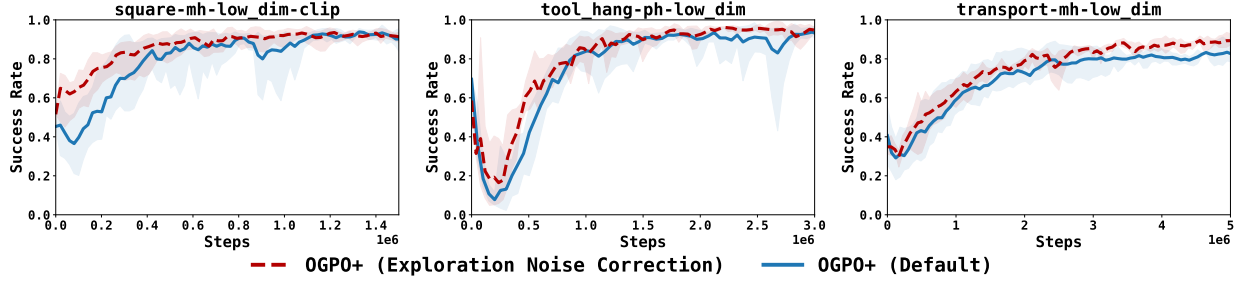


Figure 21: Comparison of ODE-to-SDE correction

F1 Diffusion Policy Policy Optimization (DPPO, Ren et al. [2024])

DPPO fine-tunes diffusion policies by applying PPO directly to the bi-level MDP introduced in Appendix D. In this construction, each inner denoising step induces an explicit (Gaussian) likelihood, enabling standard policy-gradient updates on the full trajectory in M_{BILEVEL} . **DPPO** then instantiates the PPO clipping objective on M_{BILEVEL} .

Concretely, let $\tilde{\pi}_\theta(\bar{a}_{\bar{t}} | \bar{s}_{\bar{t}})$ denote the policy on M_{BILEVEL} (i.e., the diffusion reverse transition at each denoising step). Given trajectories collected from $\tilde{\pi}_{\theta_{\text{old}}}$ and advantage estimates $\hat{A}^{\tilde{\pi}_{\theta_{\text{old}}}}$, **DPPO** maximizes the PPO clipped surrogate

$$\mathbb{E}_{(s_{\bar{t}}, a_{\bar{t}}) \sim \tilde{\pi}_{\theta_{\text{old}}}} \left[\min \left(\frac{\tilde{\pi}_\theta(a_{\bar{t}} | s_{\bar{t}})}{\tilde{\pi}_{\theta_{\text{old}}}(a_{\bar{t}} | s_{\bar{t}})} \hat{A}^{\tilde{\pi}_{\theta_{\text{old}}}}(s_{\bar{t}}, a_{\bar{t}}), \text{clip} \left(\frac{\tilde{\pi}_\theta(a_{\bar{t}} | s_{\bar{t}})}{\tilde{\pi}_{\theta_{\text{old}}}(a_{\bar{t}} | s_{\bar{t}})}, 1 - \epsilon, 1 + \epsilon \right) \hat{A}^{\tilde{\pi}_{\theta_{\text{old}}}}(s_{\bar{t}}, a_{\bar{t}}) \right) \right].$$

DPPO further uses an advantage estimator tailored to the bi-level structure: since rewards occur only at $\bar{t}(t, 0)$, it computes environment-discounted returns across t and applies an additional denoising discount across k to downweight earlier (noisier) denoising steps.

F2 Diffusion Steering Reinforcement Learning (DSRL, Wagenmaker et al. [2025])

DSRL improves a pretrained diffusion (or flow) policy without updating its weights by learning a policy over the *input noise space* while keeping the denoising dynamics fixed. Whereas a base diffusion policy π_{dp} samples an initial latent w_t from a fixed prior (typically $\mathcal{N}(0, \mathbf{I})$) to maps it to an executed action $a_{t,0}$ via a deterministic denoising chain (e.g., DDIM), **DSRL** instead formulates a *latent-action MDP* in which the fixed prior is replaced by a learnable latent policy $\pi_\psi^\mathcal{W}(w_t | s_t)$. This policy selects specific noise vectors to steer the frozen denoising process toward actions with higher expected return.

Formally, let $\pi_{\text{dp}}(s_t, w_t)$ denote the action produced by running the (frozen) denoising procedure of π_{dp} initialized at w_t , i.e., $a_{t,0} = \pi_{\text{dp}}(s_t, w_t)$. Note that if the denoising sampler is stochastic, interpret π_{dp} as inducing a conditional distribution over $a_{t,0}$ given (s_t, w_t) . This induces a latent-action transition kernel

$$P^\mathcal{W}(s_{t+1} | s_t, w_t) := P(s_{t+1} | s_t, \pi_{\text{dp}}(s_t, w_t)),$$

and **DSRL** optimizes the latent policy by maximizing the discounted return in this latent-action MDP:

$$\max_{\psi} J(\psi) := \mathbb{E} \left[\sum_{t \geq 0} \gamma^t R(s_t, \pi_{\text{dp}}(s_t, w_t)) \right], \quad w_t \sim \pi_\psi^\mathcal{W}(\cdot | s_t).$$

In practice, $\pi_\psi^\mathcal{W}$ is learned with a standard off-policy actor-critic algorithm (e.g., SAC) using transitions (s_t, w_t, r_t, s_{t+1}) collected by executing $a_{t,0} = \pi_{\text{dp}}(s_t, w_t)$ in the environment.

Optimized Variant. Our **DSRL+** variant applies best-of-N filtering over steering policy actions using the Q-functions and adds a BC-loss using the success buffer to the steering policy on top of the policy gradient loss.

F3 Expressive Policy Optimization (**EXPO**, Dong et al. [2025])

EXPO is designed to stably fine-tune *expressive* policies (e.g., diffusion/flow policies) with online RL by avoiding direct value maximization through the expressive policy parameters. Instead, **EXPO** maintains (i) a *base* expressive policy π_{base} trained with a stable imitation (supervised) objective, and (ii) a lightweight Gaussian *edit* policy π_{edit} that performs local action refinement toward higher Q-values. At interaction time, **EXPO** constructs an *on-the-fly* (OTF) policy that samples candidate actions from π_{base} , refines them with π_{edit} , and executes the candidate with the highest critic value; the same OTF selection is also used inside the TD backup.

Given $a \sim \pi_{\text{base}}(\cdot | s)$, **EXPO** samples an additive edit $\delta \sim \pi_{\text{edit}}(\cdot | s, a)$ and forms the refined action $\tilde{a} = a + \delta$. The OTF policy selects the better of the candidates according to the critic, $a^*(s) \in \arg \max_{a' \in \{a, \tilde{a}\}} Q_\phi(s, a')$. The edit policy is updated to increase the value of refined actions (with entropy regularization).

$$\max_{\pi_{\text{edit}}} \mathbb{E}_{(s,a) \sim \mathcal{D}, \delta \sim \pi_{\text{edit}}} [Q_\phi(s, a + \delta) - \alpha \log \pi_{\text{edit}}(\delta | s, a)].$$

The critic is trained by TD regression using the same OTF selection for the next-state action:

$$\min_{\phi} \mathbb{E} \left[\left(r + \gamma Q_\phi(s', a^*(s')) - Q_\phi(s, a_t) \right)^2 \right].$$

Finally, π_{base} is updated only through imitation-style regression (not direct Q-maximization), with value improvement coming from π_{edit} and the OTF selection.

Improve Variant. **EXPO+** modifies the behavior cloning term in the standard **EXPO** for the “success buffer” variant described in Section 4.2.

F4 Q-Chunking (**QC**, Li et al. [2025])

Recall that, in our notation, we use a single action a_t to decode an entire action-chunk in a the true environment, $a_{t:t+h-1}$. The **QC** algorithm proposes multiple variants. One of which, when specialized to GCPs, would require backpropagation through denoising steps, which we show leads to poor performance in Figure 25. Therefore, we opt for the other variant, which amounts to simply best-of-N inference plus behavior cloning. This variant of **QC** consists of three simple components:

- Learn a critic $Q(s, a)$, following the action-chunking conventions in Appendix A.1. Use this to train the critic via Eq. (2.3).
- Compute the Best-of-N action, by Q_{targ} , as following Eq. (4.4).
- Finally, we use a behavior cloning loss applied to past (s, a) pairs collected by the above planning mechanism.

Optimized Variant. Our **QC+** variant only applies BC loss to successful actions.

F.4.1 Q-Chunking v/s OGPO

Q-Chunking learns Q-functions that evaluate entire action chunks as atomic units, treating $Q(s, a_{1:H})$, where $a_{1:H}$ denotes the full action sequence over a horizon H . This formulation is agnostic to how the action chunk is generated—whether via a flow policy, a diffusion model, or direct regression. Policy improvement is guided using the Q-functions to rank a batch of actions and perform supervised fine-tuning (SFT) using BC loss on the Best-of-N actions. In contrast, **OGPO** explicitly leverages the iterative structure of the iterative generative policy (GCP) by computing annealed importance sampling ratios over the denoising chain Eq. (3.2). Moreover, the advantage computation evaluates the group relative Q values over the entire action chunk and the policy gradient loss propagates through *every* denoising step k . This end-to-end formulation ensures that producing a high-value action requires coherent refinement at every GCP step, rather than treating the generation process as a black box.

F.5 ReinFlow (Zhang et al. [2025b], not compared)

The ReinFlow algorithm [Zhang et al., 2025a] is nearly identical to OGPO, except that it uses a flow policy as a base policy instead of Diffusion. To get non-singular likelihood ratios, it augments the flow model with additional noise. However, their reported numbers are less sample efficient than **DPPO** (the flow sampling, however, improves *computational* efficiency), so we only use **DPPO** as a stronger baseline.

F.6 PA-RL (Mark et al. [2024], not compared)

The PA-RL Mark et al. [2024] algorithm is similar to QC, but includes an additional gradient ascent step $a' \leftarrow \nabla_a Q(s, a)$ to further improve actions. These gradient computations present a significant computational overhead, and perform best on TPU hardware. We found this method infeasible to run given our compute budget. Furthermore, given the instability of Q-gradients in non-smooth tasks [Suh et al., 2022], we conjecture this method would struggle in the contact-rich ROBOMIMIC tasks.

G Understanding Exploration Behavior of **OGPO**

This section elaborates on the exploration dynamics of **OGPO** discussed in Section 6.1. We provide visualizations that clarify how **OGPO** expands the action manifold of pretrained policy distributions while maintaining stable policy improvement.

Sample Efficiency vs. Execution Efficiency In the training dynamics of **OGPO**, we observe two colliding optimization objectives: (1) **Sample Efficiency**: Minimizing the number of environment interactions required for policy convergence, and (2) **Execution Efficiency**: Minimizing the number of timesteps the policy takes to complete a task during inference. **OGPO** excels at the former via off-policy stitching, but the latter introduces unique instabilities. The discount factor $\gamma < 1$ in the Bellman equation $Q(s, a) = r + \gamma Q_{\text{targ}}(s', a')$ creates a contraction map that conditions the policy to solve tasks as quickly as possible to maximize the expected return-to-go. This causes the IGP to generate actions that could potentially maximize the speed of achieving the goal, but do not necessarily abide by physical constraints like gravity, acceleration, and robot joint position and velocity limits. This explains the oscillations in the success rate during RL-finetuning induced by rapid policy convergence via Q functions.

Visualizing Action Distributions. Figure 13 displays UMAP embeddings of action distributions at critical states from TOOLHANG, sampled at four stages: (i) end of BC pretraining, (ii) initial RL, (iii) mid RL, and (iv) end RL. We further run the natural baselines on the PushT task and rollout 50 trajectories

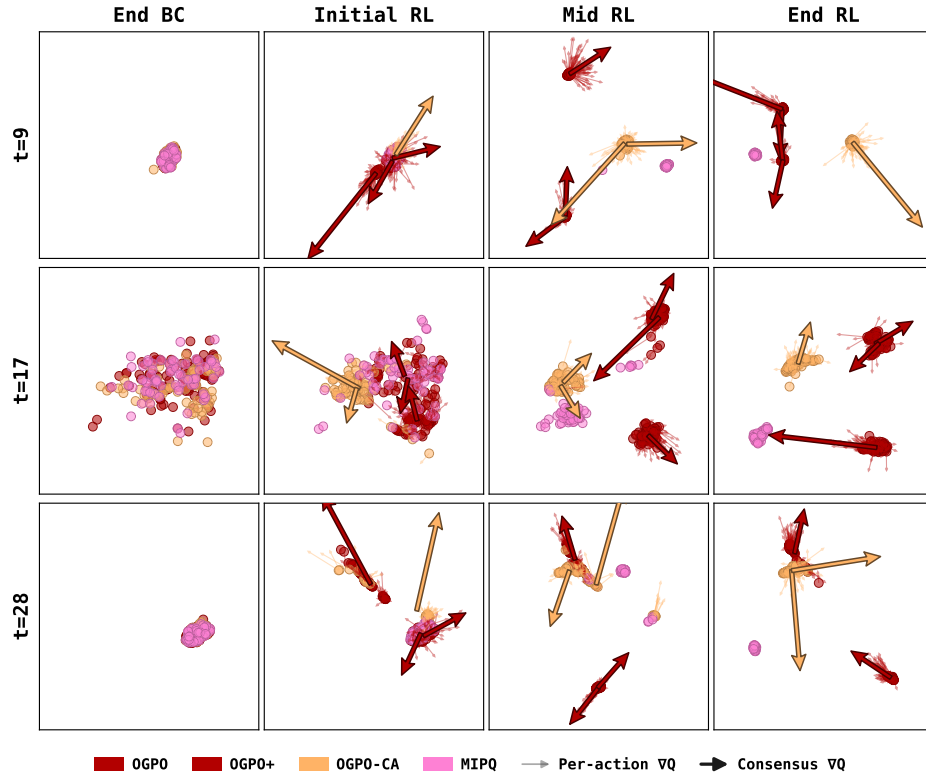


Figure 22: UMAP plot of **OGPO**, **OGPO+**, and **OGPO+CA** on ROBOMIMIC TOOLHANG

and a no-negative grad ablation of **OGPO**. We show these rollouts in Figure 15 where the dark points represent the initial actions in the trajectory through the bright yellow ones, that represent the end of the trajectory. The classical Push-T sparse rewards allow **OGPO** to exploit the TD learning objective to learn executionally efficient policies with minimal corrective actions (denoted by end-stage yellow-orange points near the Push-T handle).

1. At the end of BC, all methods produce similar action distributions, confirming that differences emerge during RL finetuning rather than from initialization.
2. **OGPO** demonstrates the multi-modal conditioning of the policy via Q-functions which can be intuitively demonstrated in Fig. 14. To test this hypothesis, we add an action compensation term $r - \Delta a_t$
3. Methods like **QC** and **DSRL** show limited manifold expansion, remaining closer to the BC initialization. **EXPO**'s residual policy facilitates support expansion but not optimal policy extraction. This can be seen by a range of corrective actions being taken near the T-shape handle.

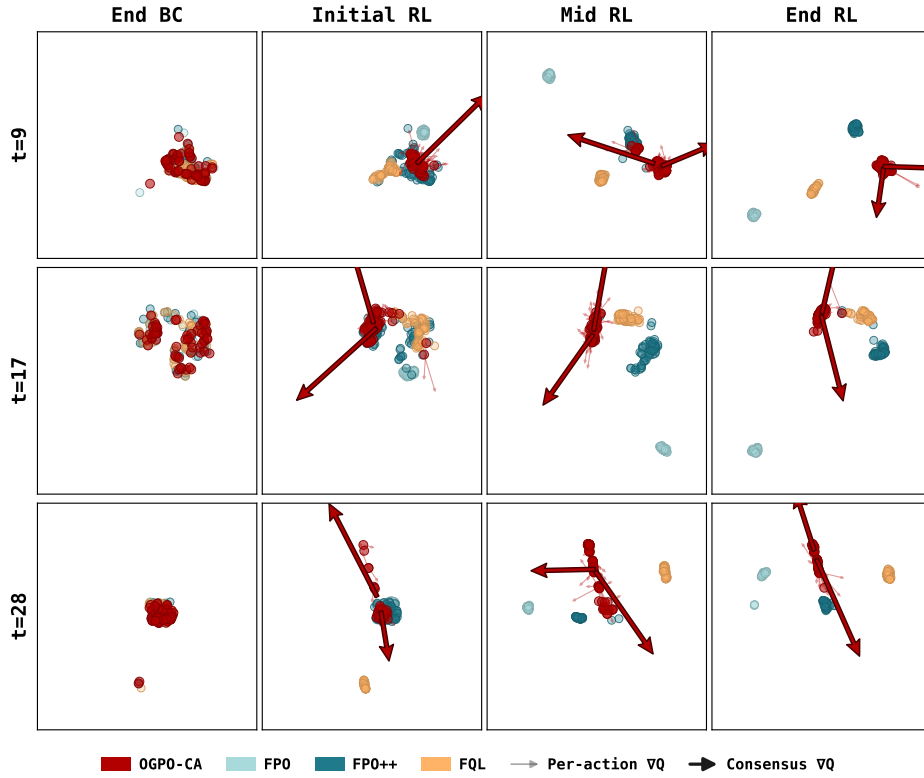


Figure 23: UMAP plot of **OGPO** comparison with various policy extraction methods on ROBOMIMIC TOOLHANG

H Ablations and Limitations of **OGPO/OGPO+**

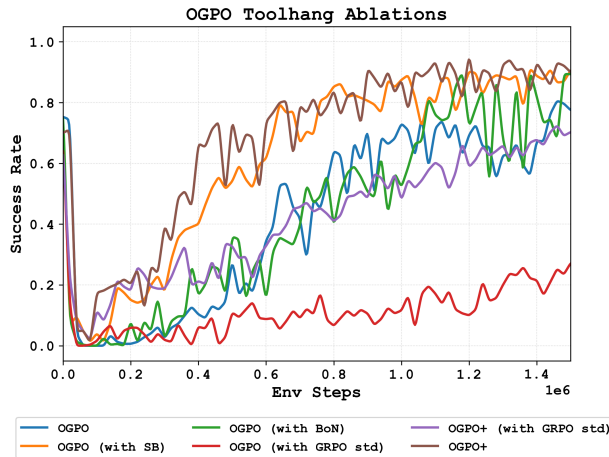


Figure 24: **OGPO** - **OGPO+** design ablations show that success buffer plays a crucial role in **OGPO+**'s performance.

H.1 **BPTT** vs **OGPO**

The most direct way to train off-policy RL policies is to perform gradient ascent on the Q-values. Although this works for simpler policy parameterizations like Gaussian [Fujimoto et al., 2018], or Squashed Gaussian [Haarnoja et al., 2018] policies, directly using Q values to sequentially backpropagate through the GCP (also referred to as *Back Propagation Through Time (BPTT)*) can be unstable [Bengio et al., 1994]. **OGPO** modifies the off-policy learning paradigm for a general class of GCPs by (1)

retaining the TD error loss for Q function updates, and (2) using Q functions as substitutes for Monte Carlo rollouts and computing relative advantages \hat{A}^G for PPO-style updates over the entire GCP chain for the policy updates.

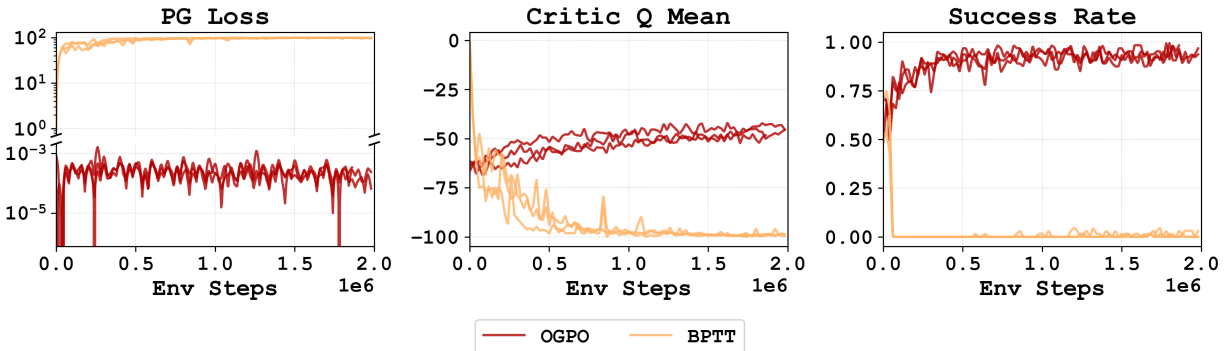


Figure 25: **BPTT** uses Q-values directly to backpropagate gradients along the entire GCP chain. This results in unstable gradients and poor convergence. In contrast, **OGPO** uses PPO-style policy gradient loss using Q-functions described Eq. (3.2). This results in stable gradients and sample-efficient convergence.

H.2 OGPO v/s OGPO+, with and without GRPO std (σ)

GRPO formulation uses group relative advantage computation similar to **OGPO**. However, the GRPO advantage uses the standard deviation of the critic ensembles to normalize the advantage values. We found this to be empirically detrimental to **OGPO**'s success. We attribute this pattern to the sensitivity of the Annealed Importance Sampling ratio ω to very large and very small advantage values. We leave an extensive empirical validation of this sensitivity as future work.

H.3 OGPO vs. OGPO+ with no-negative gradients

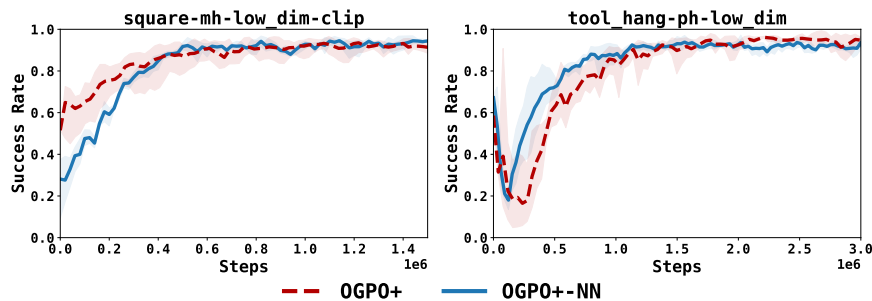


Figure 26: **OGPO+** vs **OGPO+** with no-negative gradients

H.4 OGPO vs Steering + Residual Ablation

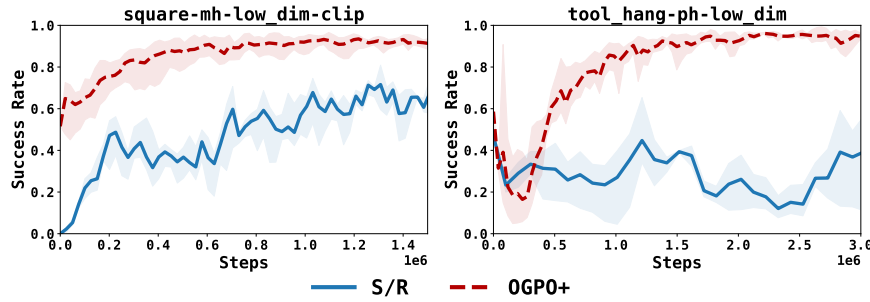


Figure 27: **OGPO+** comparison with an ablation of simultaneous steering and residual learning baseline: **S/R**

H.5 Policy Extraction Alternatives (AWR, ASPO from FPO)

OGPO separates critic learning from policy extraction: after learning Q_ϕ with the TD objective, the actor update only needs a mechanism for increasing the probability of high-advantage actions and decreasing the probability of low-advantage actions. This makes it natural to ask whether the PPO-style extraction in **OGPO** is necessary, or whether simpler weighted-regression or flow-matching objectives suffice. To isolate the effect of the extraction objective, all variants below use the same replay buffer, critic update, EMA policy $\pi_{\bar{\theta}}$, and group-relative advantages \hat{A}^G as in Eq. (3.2); only the actor loss is changed.

H.5.1 Advantage-Weighted Regression and Advantage-Weighted **OGPO**

AWR-style extraction replaces the clipped PPO ratio with weighted flow-matching regression toward samples from the reference policy. For a sampled final action $a_0 \sim \pi_{\bar{\theta}}(\cdot | s)$, we define

$$w_{\text{AWR}}(s, a_0) = \exp\left(\frac{\hat{A}^G(s, a_0)}{\beta}\right), \quad (\text{H.1})$$

where β controls how sharply the update concentrates on high-advantage samples. In our flow-policy implementation, the actor loss is not a discrete denoising-chain log-likelihood; it is a weighted conditional flow-matching objective:

$$\mathbb{L}_{\text{AWR}}(\theta) = \mathbb{E}_{s \sim \mathcal{B}, a_0 \sim \pi_{\bar{\theta}}(\cdot | s)} \left[\text{sg}(w_{\text{AWR}}(s, a_0)) \cdot \mathbb{E}_{\tau, \xi} \|v_\theta(x_\tau, \tau, s) - (a_0 - \xi)\|^2 \right], \quad (\text{H.2})$$

where $\xi \sim \mathcal{N}(0, I)$, $\tau \sim \text{Unif}(0, 1)$, and $x_\tau = \tau a_0 + (1 - \tau)\xi$. We also evaluate advantage-weighted **OGPO** (**AW-OGPO**), which preserves the same group-relative advantage computation but replaces the clipped PPO surrogate with this advantage-weighted CFM update. Empirically, these objectives are brittle on high-precision and long-horizon tasks: they can imitate high- Q samples, but do not reliably suppress bad modes when the critic is imperfect.

H.5.2 ASPO from Flow Policy Optimization

We also compare against the asymmetric trust-region objective used in Flow Policy Optimization (FPO). Instead of computing the exact denoising likelihood ratio used by **OGPO**, FPO constructs a surrogate ratio from the conditional-flow-matching loss:

$$\hat{r}_{\text{FPO}} := \exp(\hat{L}_{\text{CFM}}(\bar{\theta}; s, a) - \hat{L}_{\text{CFM}}(\theta; s, a)), \quad (\text{H.3})$$

where $\bar{\theta}$ denotes the EMA/reference policy. ASPO then applies different updates depending on the sign of the advantage. For positive advantages, it uses a PPO-style clipped objective that increases the

likelihood of good actions. For negative advantages, it uses an SPO penalty with a dead zone inside the trust region:

$$\psi_{\text{ASPO}}(\hat{r}_{\text{FPO}}, \hat{A}^G) = \begin{cases} \min(\hat{r}_{\text{FPO}}\hat{A}^G, \text{clip}(\hat{r}_{\text{FPO}}, 1 - \epsilon, 1 + \epsilon)\hat{A}^G), & \hat{A}^G \geq 0, \\ \hat{r}_{\text{FPO}}\hat{A}^G - \frac{|\hat{A}^G|}{4\epsilon} (\max(0, |\hat{r}_{\text{FPO}} - 1| - \epsilon))^2, & \hat{A}^G < 0. \end{cases} \quad (\text{H.4})$$

Thus, negative-advantage samples receive no additional SPO penalty while $\hat{r}_{\text{FPO}} \in [1 - \epsilon, 1 + \epsilon]$; the penalty only turns on once the update moves outside the trust-region boundary, and then grows quadratically in the excess violation. Compared to **OGPO**, ASPO/FPO avoids explicitly evaluating the full denoising-chain likelihood ratio, but this surrogate also weakens the connection between the extraction objective and the actual stochastic denoising process used during rollout.

Compared to **OGPO**, ASPO has the appealing property that it can be implemented directly through the CFM loss, without explicitly evaluating the full denoising-chain likelihood ratio. However, this surrogate also weakens the connection between the extraction objective and the actual stochastic denoising process used during policy rollout. In our experiments, ASPO/FPO is more competitive than pure AWR, but remains less stable than PPO-style extraction, especially on tasks where critic errors and low-value modes must be suppressed early in online learning.

I Environment Details

I.1 FRANKA-KITCHEN

The FRANKA-KITCHEN benchmark [Gupta et al., 2019] tests multi-task sequential manipulation with compositional task structure. The environment features a 9-DoF Franka robot that must manipulate 4 kitchen objects (microwave, kettle, light switch, slide cabinet) to desired goal configurations in a specific sequence. This environment is particularly challenging due to its requirement for long-horizon planning and the need to compose multiple subtasks correctly.

State and Action Spaces: The state space consists of robot joint positions, joint velocities, and object states (`state_dim` = 60). Actions are 9-dimensional continuous controls for the robot joints (`action_dim` = 9), normalized to $[-1, 1]$.

Task Horizon and Other Parameters: FRANKA-KITCHEN tasks have a medium horizon of approximately 280 timesteps. We use $\gamma = 0.99$ to account for the medium-length temporal dependencies across subtasks. The action chunk size is set to $h = 4$ to provide temporal smoothness while maintaining reactivity.

Datasets: We use three offline datasets from D4RL [Fu et al., 2020]:

- KITCHEN-COMPLETE: Complete demonstrations of all 4 subtasks in the correct sequence
- KITCHEN-MIXED: Randomized subtask orders where the desired sequence is not completed sequentially
- KITCHEN-PARTIAL: Partial subtrajectories of the desired task

Reward Structure: We use a sparse reward structure with a base reward of -7. Each successful subtask completion adds +1, with the final subtask providing +3 upon success. This yields a maximum reward of 0 for completing all subtasks.

I.2 Robomimic

The ROBOMIMIC benchmark [Mandlekar et al., 2021] provides high-precision manipulation tasks that test fine-grained control and multi-step reasoning. We evaluate on three of the most challenging tasks that represent different aspects of real-world manipulation:

Square (SQUARE): A medium-horizon fine-grained insertion task requiring precise alignment and insertion of a square peg. This task tests contact-rich manipulation with tight tolerances.

- `state_dim`: 14 (robot end-effector pose, object pose)
- `action_dim`: 7 (6D end-effector control + gripper)
- Horizon: 400 timesteps
- $\gamma = 0.99$
- Action chunk size: $h = 4$
- Dataset: Multi-Human (MH) mixed proficiency

Tool Hang (TOOLHANG): A long-horizon, highly-precise multi-step insertion task requiring the robot to grasp a tool and hang it on a rack. This task demands both coarse positioning and fine-grained alignment across multiple phases.

- `state_dim`: 14
- `action_dim`: 7
- Horizon: 700 timesteps
- $\gamma = 0.995$ (higher due to longer horizon)
- Action chunk size: $h = 8$ (larger chunks for smoother long-horizon execution)
- Dataset: Proficient-Human (PH), BC stopped at 50% success rate

Transport (TRANSPORT): A bi-manual, multi-step, long-horizon object transfer task where two robot arms must coordinate to transport an object. This tests both individual arm control and bi-manual coordination.

- `state_dim`: 28 (dual arm configuration)
- `action_dim`: 14 (7 per arm)
- Horizon: 700 timesteps
- $\gamma = 0.995$ (higher due to longer horizon)
- Action chunk size: $h = 8$
- Dataset: Multi-Human (MH) mixed proficiency

Reward Structure: All Robomimic tasks use sparse rewards: -1 for each non-successful step, with the final successful step returning 0.

Note on Hyperparameters: The different gamma values reflect the relationship between discount factor and task horizon. Longer horizon tasks (TOOLHANG, TRANSPORT) require larger gamma (0.995) to properly credit distant actions, while medium-horizon tasks (SQUARE) use smaller gamma (0.99). Similarly, longer tasks benefit from larger action chunks ($h = 8$) for smoother execution. Importantly, both gamma and chunk size are independent of action dimensionality.

I.3 Adroit Hand

The Adroit Hand benchmark tests dexterous manipulation with a 24-DoF anthropomorphic robotic hand performing high-precision, contact-rich tasks. This environment is particularly challenging due to the high-dimensional action space, under-actuated dynamics, and the need for coordinated finger movements.

We evaluate on four standard tasks:

- `AdroitHandDoor-v1`: Door opening requiring articulated finger coordination to grasp and turn a handle
- `AdroitHandHammer-v1`: Hammering a nail with precise force control and wrist articulation
- `AdroitHandPen-v1`: In-hand pen reorientation requiring complex finger gaiting
- `AdroitHandRelocate-v1`: Object relocation requiring coordinated grasping and translation

State and Action Spaces:

- `state_dim`: 45 (24 joint positions + 24 joint velocities + object state)
- `action_dim`: 24 (continuous control for each DoF)
- Actions normalized to $[-1, 1]$

Task Horizon and Temporal Parameters:

- Horizon: 200 timesteps (medium-horizon tasks)
- $\gamma = 0.99$
- Action chunk size: $h = 4$ for stabilized policy execution

Datasets: We use expert demonstration datasets provided via the D4RL/Minari interface for pre-training the base policy.

Evaluation: Following prior work, we evaluate performance using the normalized return provided by the environment, scaled to $[0, 100]$.

I.4 LIBERO

The LIBERO benchmark [Liu et al., 2023] tests vision-based, language-conditioned manipulation for multi-task learning and generalization. Unlike the previous environments, which use state-based observations, LIBERO provides pixel observations and requires following natural-language instructions, thereby testing both visual understanding and instruction-following capabilities.

Observation and Action Spaces:

- Observations: RGB images ($128 \times 128 \times 3$ pixels)
- `action_dim`: 7 (6D end-effector control + gripper)
- Actions normalized to $[-1, 1]$

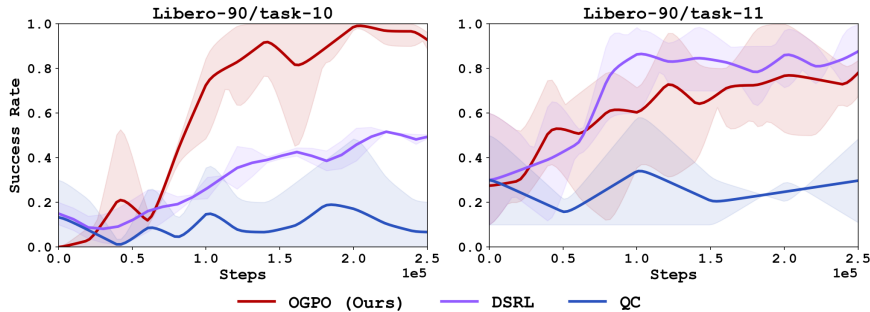


Figure 28: We compare **OGPO** with **DSRL** and **QC** on pixel-based observations and natural language guidance tasks from the LIBERO benchmark

Task Structure: LIBERO features procedurally generated tasks with natural language instructions. Tasks require understanding spatial relationships and object attributes from both visual and linguistic modalities.

Reward Structure: All Libero tasks use sparse rewards: -1 for each non-successful step, with the final successful step returning 0.

Task Horizon and Temporal Parameters:

- Horizon: 1000 timesteps (long-horizon tasks)
- $\gamma = 0.999$ (for **OGPO**, **DSRL**), 0.99 (for **QC** since we found this leads to better performance)
- Action chunk size: $h = 8$

Training and Evaluation Setup: The base policy is trained on demonstrations from 10 tasks ($\text{task_id} \in \{0, \dots, 9\}$) in the Libero-90 dataset and evaluated on 2 unseen downstream tasks ($\text{task_id} \in \{10, 11\}$) to test generalization capabilities. This setup explicitly tests the ability to transfer learned manipulation skills to novel task descriptions and object configurations. Since LIBERO is a language-conditioned benchmark, for both the actor and critic, we follow a widely used design from prior work [Walke et al., 2023, Nakamoto et al., 2024]: language instructions are first processed by a frozen MUSE encoder [Yang et al., 2019] and then passed to an IMPALA encoder [Espenholt et al., 2018] with FiLM conditioning [Perez et al., 2018].

J Hyper-parameters and Initialization

J.1 Initialization and Warm Starting

OGPO accommodates two primary settings based on data availability, each with corresponding algorithmic choices for initialization. **Setting 1: Offline data available.** When an offline dataset \mathcal{D}_{off} is available, we pre-train our policy $\bar{\pi}_{\theta}^{\text{BC}}$ on \mathcal{D}_{off} using the appropriate BC loss. The `use_offline` flag is toggled `True`, enabling offline data sampling reuse determined by the ratio r_{offline} .

Setting 2: No offline data (online-only). We finetune a pre-trained IGP with *no* additional demonstration data which has some small but non-trivial base success rate ($>10\%$). The `use_offline` flag is toggled `False`.

In both settings, the online replay buffer $\mathcal{D}_{\text{roll}}$ is initialized with N_{warmup} $\bar{\pi}_{\theta}$ rollouts, where $\bar{\pi}_{\theta} \leftarrow \bar{\pi}_{\theta}^{\text{BC}}$. Finally, we initialize an ensemble of Q-functions $Q_{\phi_{1,\dots,M}}$ with random weights and, importantly, find that no offline RL pretraining yields the highest sample efficiency. We defer the details of the offline RL ablations to Algorithm 3.

J.2 Hyperparameters

In this section, we list all the hyper parameters we use for **OGPO** across different benchmarks. Table 2 shows the maximum episode lengths we use for each environment.

Environment	Max Episode Length
square	400
transport	800
tool_hang	1000
kitchen (all)	600
adroit (all)	200

Table 2: Environment maximum episode lengths

We first list the common **OGPO** hyper parameters. Unless otherwise stated, these remain constant throughout all our experiments. These are in Table 3.

Parameter	Default Value
lr	3e−4
actor_lr	3e−4
critic_lr	3e−4
ppo_lr	4.5e−5
tau	0.05
actor_tau	0.05
discount	0.99
batch_size	256
ppo_batch_size	256
actor_hidden_dims	(512, 512, 512, 512)
value_hidden_dims	(512, 512, 512, 512)
num_qs	10
q_agg	mean
subsample_bon	True
flow_steps	10
grp_num_samples	32
clip_epsilon	0.01
entropy_coeff	0.0
bc_coeff	1.0
constant_noise_std	0.01
actor_scheduler	cosine
critic_scheduler	constant
actor_warmup_steps	2000
actor_decay_steps	50000
actor_end_value	2e−5
critic_warmup_steps	500
critic_decay_steps	5000
critic_end_value	0.0
actor_weight_decay	0.0
critic_weight_decay	1e−5
horizon_length	4
policy_type	flow

Table 3: OGPO agent default hyperparameters.

In Table 4, we list down all ROBOMIMIC specific hyper-parameters that are used for our experiments.

Hyperparameter	SQUARE	TOOLHANG	TRANSPORT
Training Steps			
offline_steps	500,000	500,000	1,000,000
online_steps	2,000,000	3,000,000	6,000,000
start_training	20,000	25,000	40,000
RL Hyperparameters			
horizon_length	4	8	8
discount	0.99	0.999	0.999
tau	0.05	0.05	0.05
utd_warmup	1	1	1
utd_online	1	1	1
Q-Network			
num_qs	10	10	10
q_agg	mean	mean	mean
subsample_bon	True	True	True
best_of_n	8	8	8
value_hidden_dims	(512,512,512,512)	(512,512,512,512)	(512,512,512,512)
BC Regularization			
use_bc_regularization	True	True	True
bc_coeff	1.0	1.0	1.0
pg_coeff	1.0	1.0	1.0
clip_bc (atmost 50% success rate)	True	True	False

Table 4: OGPO hyperparameters for Robomimic environments.

In Table 5, we list all hyper parameters we use for the various FRANKA-KITCHEN environments.

Hyperparameter	KITCHEN-COMPLETE	KITCHEN-MIXED	KITCHEN-PARTIAL
Training Steps			
offline_steps	1,000,000	1,000,000	1,000,000
online_steps	3,000,000	3,000,000	3,000,000
RL Hyperparameters			
horizon_length	4	4	4
discount	0.99	0.99	0.99
tau	0.05	0.05	0.05
utd_warmup	1	1	1
utd_online	1	1	1
Q-Network			
num_qs	10	10	10
q_agg	mean	mean	mean
subsample_bon	True	True	True
best_of_n	8	8	8
BC Regularization			
use_bc_regularization	True	True	True
bc_coeff	0.1	0.1	0.1
clip_bc	False	False	False

Table 5: OGPO hyperparameters for FRANKA-KITCHEN

In Table 6, we list all hyper parameters we use for the various FRANKA-KITCHEN environments.

Hyperparameter	Door-v1	Pen-v1	Hammer-v1	Relocate-v1
Training Steps				
offline_steps	50,000	50,000	50,000	50,000
online_steps	500,000	500,000	500,000	500,000
RL Hyperparameters				
horizon_length	4	4	4	4
discount	0.95	0.95	0.95	0.95
tau	0.05	0.05	0.05	0.05
utd_warmup	1	1	1	1
utd_online	4	4	4	4
Q-Network				
num_qs	10	10	10	10
q_agg	min	min	min	min
subsample_bon	False	False	False	False
best_of_n	8	8	8	8
BC Regularization				
use_bc_regularization	True	True	True	True
bc_coeff	1.0	1.0	1.0	1.0
clip_bc	True	True	True	True

Table 6: OGPO hyperparameters for Adroit.

In Table 7, we list all hyperparameters we use for the Libero environments.

Hyperparameter	Libero
Training	
offline_steps	50,000
online_steps	250,000
actor_tau	0.001
batch_size	64
constant_noise_std	0.01
grpo_num_samples	8
RL Hyperparameters	
horizon_length	8
discount	0.999
tau	0.05
utd_online	1
Q-Network	
num_qs	10
q_agg	mean
encoder	impala_small
value_hidden_dims	(128, 128, 128)
BC Regularization	
use_bc_regularization	False
offline_ratio	0

Table 7: OGPO hyperparameters for Libero.